THE ASTROPHYSICAL JOURNAL SUPPLEMENT SERIES, 41:435–450, 1979 November

STRUCTURE AND ORIGIN OF S0 GALAXIES. I. SURFACE PHOTOMETRY OF S0 GALAXIES*

DAVID BURSTEIN†
Board of Studies, Astronomy and Astrophysics, University of California, Santa Cruz; and
Department of Terrestial Magnetism, Carnegie Institution of Washington
Received 1979 February 7; accepted 1979 April 4

ABSTRACT

Two-dimensional photographic surface photometry, in the *B* passband, is presented for 18 S0 galaxies and one elliptical, NGC 3379. Isophotal maps and major- and minor-axis profiles are given for these galaxies. Both an internal evaluation and an external evaluation of these data indicate that they are (overall) accurate to about 2% from a surface brightness of 18 to 26 mag arcsec^{-2}. Comparisons of the present photometry are made with that of a number of other observers, and possible serious systematic errors in earlier work are pointed out.

The luminosity structure of S0 disks can vary considerably; of the 16 ordinary S0's in this sample, five have subtle nonaxisymmetric peculiarities in their disks. Since the S0's in this sample were chosen primarily for their "normality," it is possible that about one-half of all S0's have nonaxisymmetric phenomena (besides bars) in their disks.

The observed major-axis disk profiles are basically exponential, but almost all of the disks deviate in one way or another from being exactly exponential. These deviations usually take the form of humps or bumps in the disk luminosity profile that can vary both in length scale and in amplitude.

Subject headings: galaxies: photometry — galaxies: structure

I. INTRODUCTION

S0 galaxies occupy a unique position among the classes of normal galaxies; they have a generally old stellar population and little observable gas, like ellipticals (e.g., the survey of Balick, Faber, and Gallagher 1976), but they also have a visible disk with an exponential luminosity distribution, like spirals (Freeman 1970; Sandage, Freeman, and Stokes 1970).

The various theories that have been proposed for the origin of S0 galaxies can be divided into two main groups: (*a*) In the "parallel-sequence" theories, S0's are thought to be galaxies which were once spirals but which are now gas-free. Examples of such theories include those in which a spiral is stripped of gas through interaction with an intracluster medium or by collision with another galaxy (originally suggested by Baade and Spitzer 1951; more recently suggested by Gunn and Gott 1972; van den Bergh 1976; Binney and Silk 1978), and those in which certain spirals convert gas to stars much more efficiently than do other spirals (e.g., Strom and Strom 1978). (*b*) In the "transition" theory, ellipticals and S0's are thought to form a true continuum of galaxies, the common characteristic of which is the ability to keep themselves clean of gas.

Most of the parallel-sequence theories view the continuity of the Hubble sequence as being partly the result of postformation interactions of galaxies with their environment; the transition theory views the Hubble sequence as intrinsic, with galaxy properties determined by the manner in which a galaxy is formed.

* *Lick Observatory Bulletin*, No. 827.

† Guest Investigator at the Hale Observatories.

In their simpler forms, parallel-sequence theories predict that the frequency of disk-to-bulge ratios ($\mathscr{D}/\mathscr{B}$) among S0's will be parallel to that among spirals, and that the detailed structural characteristics of S0's and spirals should be similar. While some previous studies of $\mathscr{D}/\mathscr{B}$ among spirals and S0's (Sandage *et al.*; Freeman 1970) suggest that the former is true, another study (Yoshizawa and Wakamatsu 1975) implies that $\mathscr{D}/\mathscr{B}$ are smaller for S0's than for spirals.

Unfortunately, many of the data for the S0 galaxies used in these investigations were taken from surface photometry with a wide variation in resolution and accuracy (see § IV), so that it is difficult to evaluate the reliability of their results.

The present surface photometry program was initiated primarily to measure the $\mathscr{D}/\mathscr{B}$ of a representative cross section of S0 galaxies and to detail the two-dimensional structure of S0 disks. These data can then be compared with similar data for spirals. Several edge-on S0's were specifically included in this sample since the dust-free character of S0's offered the possibility of observing the light distribution perpendicular, rather than parallel, to the plane of the disk.

This paper presents the basic surface photometry data for the program S0 galaxies, along with general comments about S0's as a class. Section II describes how the S0's in this program were selected, and the reduction procedure for the surface photometry is summarized in § III. The present data are compared with the results of other investigations in § IV, and comments about the structure of S0 disks are given in § V.

The quantitative analysis of the surface photometry data presented in this paper will be made in subsequent papers in this series.

II. SELECTION OF GALAXIES

In the selection of the program objects, an effort was made to include a representative sample cross section of S0 galaxies, subject to the following constraints. They should (i) be no more distant than the Virgo cluster; (ii) be in groups or clusters with known distances; (iii) be ordinary S0's without a prominent bar; (iv) have a range of inclination to the line of sight, including highly inclined systems; and (v) have a wide range of apparent $\mathscr{D}/\mathscr{B}$ as determined by visual inspection and from available surface photometry (Liller 1960, 1966; Sérsic 1968; Benedict 1971).

Of the approximately 40 galaxies which satisfied criteria (i)–(iii) (and were in a part of the sky accessible to Mount Hamilton), 17 S0's were finally chosen. These 17 included about six galaxies in each of three inclination categories: face-on, intermediate, and edge-on. Those chosen covered the full range of available $\mathscr{D}/\mathscr{B}$ estimates. The well-studied elliptical galaxy NGC 3379, along with its companion SB0 galaxy NGC 3384, were also included in the sample as checks on the accuracy of the photometry. General information on the final 19 galaxies selected is given in Table 1.

III. PHOTOGRAPHIC DATA REDUCTION

A total of five plates taken in the photographic B passband (103a-O emulsion +2 mm GG 13 filter) were obtained for each galaxy. Three plates of exposure length 13, 30, and 45 minutes were taken with the Crossley 90 cm telescope (scale 38″.63 mm^{-1}), and two plates of exposure length 6 and 18 minutes were taken with the 1.2 m Palomar Schmidt telescope (scale 67″.2 mm^{-1}). The Crossley plate scale is large enough to detail all but the very inner nuclear regions (radii $r < 3''$) of the program galaxies, while the large field of the Schmidt permitted an adequate definition of the background sky level.

The details of the surface photometry reduction procedure are given elsewhere (Burstein 1978, 1979), so only a brief summary will be given here.

All plates were developed in a Mount Wilson–type tray rocker (Miller 1971) in D-19 developer for 4 minutes at 20° C. Two spot sensitometers, one each at the Crossley (with 13 spots, spaced in intervals of $\sqrt{2}$ in intensity) and at Mount Palomar (with 12 spots), were used to place calibration spot "sets" on the plates taken with the respective telescopes. Additional spot sets were placed on separate plates with the Palomar sensitometer, both to supplement the calibrations on the telescope exposures and to substitute for the absence of calibrations on nine plates taken with the Schmidt during 1975 April. All Palomar plates were exposed to the calibration spots on the dome floor, while the Crossley calibrations were put on plates in the darkroom. All but the 13 minute Crossley plates had calibration exposure times within a factor of 1.2 of that of the telescope exposures; the 13 minute exposures had 25 minute calibrations. Most plates were developed 12–18 hours after exposure to allow each plate to age the same amount of time to within 25%. A GG 13 filter was used with the sensitometers, but no attempt was made to change the color temperature of the calibration lamps (since the characteristic curve of the 103a-O emulsion is not very sensitive to changes in effective wavelength [cf. Eastman Kodak Co. 1973 and results from internal tests]).

Of the 80 plates available for surface photometry (five plates per field, 16 fields, with three fields containing two galaxies each), 78 were used; galaxies on the two unusable plates are noted in Table 1.

The plates were scanned in two-dimensional arrays with the photometric data systems (PDS) microdensitometer at UC Berkeley. An "inner" data array, consisting of 256 × 256 pixels, each pixel 20 μm square, was generated for each galaxy; an "outer" array, consisting of about 175 × 175 pixels, each pixel 200 μm square, was generated for each plate.

Preliminary testing showed that calibrations from different plates (even those taken over a period of time) could be reliably combined to produce a more accurate definition of the characteristic curve (see Burstein 1979 for details). Naturally defined spot "groups," each consisting of from two to 18 individual spot "sets," were used to generate average characteristic curves, which were then applied to the plates in the respective groups. This procedure has several advantages over using only the calibrations on the individual plates. A least-squares fit was made, using these spot groups, to transform density (D) to intensity (I) via the equation (cf. Kormendy 1977; de Vaucouleurs 1968)

$$\log I = \sum_{i=0}^{n} a_i(\log \omega)^i\,, \quad \text{where } \omega = 10^D - 1$$

$$\text{or} \quad \omega = \frac{1}{T} - 1\,,$$

with n typically 5–7.

The sky background was subtracted from each plate in the following manner (cf. Jones *et al.* 1967): After conversion to intensity, a histogram of data values, with a resolution of 400 μm, was made for each outer array. Maximum and minimum values for the sky were chosen from this histogram (Burstein 1979); in addition, areas of arbitrary size, including a generously large area around the galaxy (or galaxies), could be excluded from the fit. All data that satisfied both criteria of value and position were fitted with a two-dimensional polynomial of either first or second order.[1] Sky was subtracted from the inner array by scaling the sky intensity using the overlap of the inner to the outer array.

[1] A second-order fit was used for the Crossley plates because of the presence on many plates of a background gradient. This gradient was due to scattered ambient night sky + stellar light in the Crossley camera and was therefore treated as additional background light.

TABLE 1

GENERAL DATA FOR PROGRAM GALAXIES

NGC (1)	R.A. 1950.0 (2)	Decl. (3)	Type (4)	Dist. (5)	B_T (6)	V_0 (7)	P.A. (8)	Z.P. Qual. (9)
3379	$10^h45^m11^s.3$	12°50′48″	E1	16	10.20	756	60.0	A
3384	10 45 38.7	12 53 41	SB(s)0$^-$	16	10.87	642	49.0	A
3489	10 57 40.0	14 10 15	SAB(rs)0$^+$	12	11.15	577	74.3	A
4111	12 04 30.5	43 20 43	SA(r)0$^+$	16	11.50	841	150.5	B
4150	12 08 01.3	30 40 47	SA(r)0^0	7.6	12.45	235	148.0	C
4203	12 12 34.1	33 28 33	SAB0$^-$	19	11.55	1007	8.4	B
4270	12 17 15.4	05 44 31	S0	43	13.10	2233	108.1	B
4281	12 17 48.4	05 39 51	S0$^+$	43	12.21	2488	85.6	B
4324	12 20 32.5	05 31 36	SA(r)0$^+$	22	12.55*	1602	55.4	C
4350	12 21 26.4	16 58 11	SA0	22	11.90	1121	28.9	B
4377	12 22 40.6	15 02 28	SA0$^-$	22	12.65	1281	175.5	B
4382	12 22 53.2	18 28 03	SA(s)0$^+$p	22	10.10	718	79.5†	A
4429	12 24 54.1	11 23 05	SA(r)0$^+$	22	11.10	1029	99.2	A
4459‡	12 26 28.3	15 14 20	SA(r)0$^+$	22	11.35	1039	103.0	A
4474‡	12 27 21.7	14 20 40	S0p	22	12.6	1455	80.0	C
4526	12 31 30.4	07 58 33	SAB(s)0^0	22	10.58	355	110.8	B
4570	12 34 20.8	07 31 22	S0	22	11.7	1635	160.4	C
4578	12 34 58.7	09 49 48	SA(r)0^0	22	12.27	2197	35.2	B
4762§	12 50 25.5	11 30 05	SB(r)0^0	22	11.12	878	31.4	B

* From Harvard magnitude m_c.

† See table notes.

‡ 30 minute Crossley plate not used.

§ 18 minute Palomar plate not used.

NOTES TO TABLE 1

Col. (1).—NGC designation.

Col. (2).—Right ascension, 1950.0, from Dressel and Condon 1976.

Col. (3).—Declination, 1950.0, from Dressel and Condon 1976.

Col. (4).—Morphological type from RCBG II.

Col. (5).—Distance, in Mpc, to galaxy as determined from mean velocity of the group or cluster to which the galaxy belongs, with $H_0 = 50$ km s^{-1} Mpc^{-1}.

Col. (6).—Total apparent magnitude B_T taken from RCBG II for all galaxies except NGC 4324, for which the Harvard magnitude (as corrected in RCBG II) is used.

Col. (7).—Radial velocity of the galaxy V_0 corrected for motion relative to the Local Group, as in RCBG II.

Col. (8).—Position angle of the major axis of the galaxy relative to the Crossley and the Palomar scans. The absolute accuracy of these angles is about 1° except for NGC 3379, which was measured in error at a P.A. = 60°, or 10° away from the true major axis. (Cf. Miller and Prendergast 1962. This P.A. difference has a negligible effect on the profile, as explained in n. 2 of the text.) The accuracy of the P.A. relative to the scans themselves is less than 0°.5. The P.A. for NGC 4382 is the line joining the center of this S0 to the center of its neighbor, NGC 4394.

Col. (9).—Quality of the zero point of the luminosity profile for each galaxy. Code A denotes a probable error of less than 0.1 μ; code B denotes an error of 0.1–0.2 μ; code C denotes an error of greater than 0.2 μ.

COMMENTS ON THE S0 GALAXIES IN TABLE 1

NGC 3384.—Owing to its angular orientation, the bar in this galaxy is not apparent in the major-axis profile, but it is noticeable in the minor-axis profile (see also Barbon *et al.* 1975).

NGC 3489.—Has an unusually shaped bulge. It is described in § V*b*.

NGC 4111.—Highly inclined to the line of sight (edge-on). Both the isophotal map and the major-axis profile show evidence of a prominent lens/bar from r = 12″–24″ on the major axis. For r > 24″ the remaining profile of the disk curves downward in a (μ_B, r)-plot. A star is superposed on the southeast side of the major axis at r = 70″.

NGC 4150.—Intrinsically faintest S0 in this sample; NGC 4150 and NGC 404 are two of the faintest known S0's.

NGC 4203.—Has a relatively smooth luminosity distribution. Several stars are found within 1′ of the center; a neighboring bright star disturbs the outer part of the northern part of the major axis. This is the one true S0 in this sample that has been detected in 21 cm emission (Balick *et al.* 1976), making it one of the reddest S0's or ellipticals with detected H I gas.

NGC 4270.—Is in a group with NGC 4281 and has a warped outer disk, as seen on long-exposure plates. It is described in § V*b*.

NGC 4281.—A moderately inclined galaxy, with a dust lane which modifies the inner parts of the major- and minor-axis profiles.

NGC 4324.—Probably a misclassified S0/a or early Sa. See the discussion in § V*b*.

NGC 4350.—Forms an optical pair with its neighbor, NGC 4340, but there is no evidence in the isophotal maps of a tidal interaction between the two galaxies. The major-axis profile of NGC 4350 is primarily exponential, with a small change in disk slope at r = 25″.

NGC 4377.—A relatively faint S0 in the Virgo cluster in front of a small distant cluster. The redshift of the brightest member of this background cluster (23″ northeast of the center of NGC 4377) is approximately 13,200 km s^{-1} (as measured with the Lick 3 m image tube scanner [ITS]) compared to 1270 km s^{-1} for NGC 4377 (RCBG II; confirmed with the ITS). This background elliptical also matches the position of the radio continuum source around NGC 4377, as given in the catalog of Haynes *et al.* 1975.

NGC 4382.—Discussed in § V*b* along with its companion, NGC 4394. Along with NGC 4526, NGC 4382 is one of the brightest S0's in the Virgo cluster and one of the brightest known S0's.

NGC 4429.—Discussed in § V*b*. A bright star disturbs the northern part of the galaxy profile, and a strong dust lane disturbs the galaxy profile near the center.

NGC 4459.—Has a dust lane close to the nucleus and a star at r = 20″ along the major axis. Another star disturbs the outer southeast major-axis profile, as marked in Fig. 1.

NOTES TO TABLE 1—*Continued*

NGC 4474.—Appears more inclined to the line of sight on a short-exposure than on a long-exposure plate. The bulge luminosity distribution is exponential-like to $r = 10''$ along the major axis. The minor-axis profile shows some evidence of a bar. The light distributions of the bulge and of the disk do not merge smoothly but come together sharply at $r = 10''$ on the major axis.

NGC 4526.—Has spiral-type distortions, which are shown in Fig. 4 and described in § V*b*. Along with NGC 4382, NGC 4526 is one of the brightest S0's in the Virgo cluster and one of the brightest known S0's.

NGC 4570.—Is highly inclined to the line of sight. Although visually similar to NGC 4111 (cf. Fig. 2), NGC 4570 does not possess a prominent lens/bar. A star is superposed on the southeast part of the major axis at $r = 40''$.

NGC 4578.—Has a very smooth, regular light distribution. The halo of a star which disturbs the outer southeast part of the major axis is marked in the profiles in Fig. 1.

NGC 4762.—Is one of the thinnest, if not the thinnest, S0's known (Sandage 1961), and it appears to be tidally interacting with a nearby galaxy, NGC 4754. NGC 4762 has the most peculiar major-axis light distribution of any S0 in this sample. Three distinct plateaus in the major axis are seen, corresponding to an inner bar/lens, an outer disk (?), and the outer tidal distortion. All plateaus are visually discernible in a photograph. A more thorough investigation of NGC 4762 will be given elsewhere (Burstein *et al.* 1979).

A conservative estimate of the accuracy of the sky background levels determined in this manner appears to be no more than 0.5% of the sky (Burstein 1979). To further facilitate data handling by a small computer, inner and outer data arrays of the Crossley and Palomar plates were summed separately, with weights, to produce four final arrays per galaxy (i.e., an inner and outer "Crossley" sum of three data arrays, and an inner and outer "Palomar" sum of two data arrays). The Crossley to Palomar comparison is a useful assessment of the internal quality of the data since plates from the same telescope will probably have similar systematic errors.

IV. S0 BRIGHTNESS PROFILES: COMPARISON WITH OTHER DATA

The brightness profiles presented here were produced by a two-dimensional interpolation routine that projects a pixel of the same resolution and spatial orientation as the array pixels (i.e., either a 20 or a 200 μm square) at the designated position on the array. Thus the Crossley inner data are interpolated with a resolution of 20 μm ($= 0''.77$) in $1''$ increments; Crossley outer data with 200 μm ($= 7''.73$) resolution every $10''$; Palomar inner data with 20 μm ($= 1''.34$) resolution every $2''$; and Palomar outer data with 200 μm ($= 13''.4$) resolution every $15''$.

The data along the major and the minor axes for the 18 S0's and the major axis of NGC 3379 are tabulated in Table 2, and the S0's are plotted in Figure 1 as μ_B versus r. (The luminosity profile for NGC 3379, an elliptical, is presented elsewhere [Burstein 1978].) The data presented are as observed on the major and minor axes; no smoothing or modeling of the data has been done, except as specified above.

The magnitude zero point for each galaxy was obtained by using all available photoelectric data, and either by integrating the Crossley inner (summed) array within the appropriate size apertures or, in the cases of NGC 3379 and 3384, by comparing to the photoelectric profiles of Burkhead and Kalinowski (1974). In most cases the zero point should be good to ± 0.1 mag as judged by the internal agreement of the zero points determined from several different photoelectric observations for each galaxy. Estimates of the accuracy of the zero points for each galaxy are given in Table 1. Each of the other three (summed) arrays was then normalized in surface brightness to match the Crossley inner data.

These data were purposely not averaged in ellipses or in sections of an ellipse. Such a procedure would increase the signal-to-noise ratio at low light levels, but it would also smear out fine details. Furthermore, S0's apparently consist of at least two separate components, bulge and disk, each with its own spatial symmetries. If one wishes to study the individual components in such composite systems, then averaging around simple elliptical-like curves does not have even theoretical validity since the "elliptical" isophotes of all but the most face-on galaxies cannot be simply related to the major-axis profile in the fundamental plane of the galaxy.

Because averaging in ellipses was not done, the major- and minor-axis profiles become too noisy for $\mu_B > 26.5\ \mu$ (μ is mag arcsec^{-2}). However, for the purposes of this study, a cutoff brightness level of $\mu_B = 26.3\ \mu$ adequately defines the overall structure of the program galaxies.

Figure 2 (Plates 23–27) presents the data in two-dimensional form, with a copy of a short-exposure Crossley plate, the Crossley inner array (summed), and the Palomar (or Crossley) outer array (summed). As is evident on the outer arrays, bright star profiles can extend quite far on a plate at low light levels and overlap a galaxy image some distance away (e.g., NGC 4324, where the image of a star, $m_B = 7$, has a radius of about $10'$ at $\mu_B = 27\ \mu$). In addition, many galaxies have relatively fainter stars that are either inside the galaxy inner envelope (e.g., NGC 4382, 4203) or interfere with the outer envelope (e.g., NGC 4526, 4429). Stars of the former type are noted on the brightness profiles. Stars of the latter type are noticeable only as smooth systematic deviations in a galaxy profile at faint light levels and are also noted. Whenever possible, the profile given for the affected region is that of the uncontaminated side. A full treatment of the problems caused by extended stellar profiles was not feasible with the data reduction facilities available.

From the data plotted in Figure 1, one sees that the Crossley and the Palomar data agree internally to $\pm 0.05\ \mu$ to $\mu_B \approx 22\ \mu$ (in the mean), increasing to about 0.1–0.15 μ near the cutoff at $\mu_B = 26.3\ \mu$.

However, the best check on the accuracy of the data is a comparison with other reliable observations of the same galaxies. NGC 3379 and 3384 were included in this program for this purpose. Comparisons between

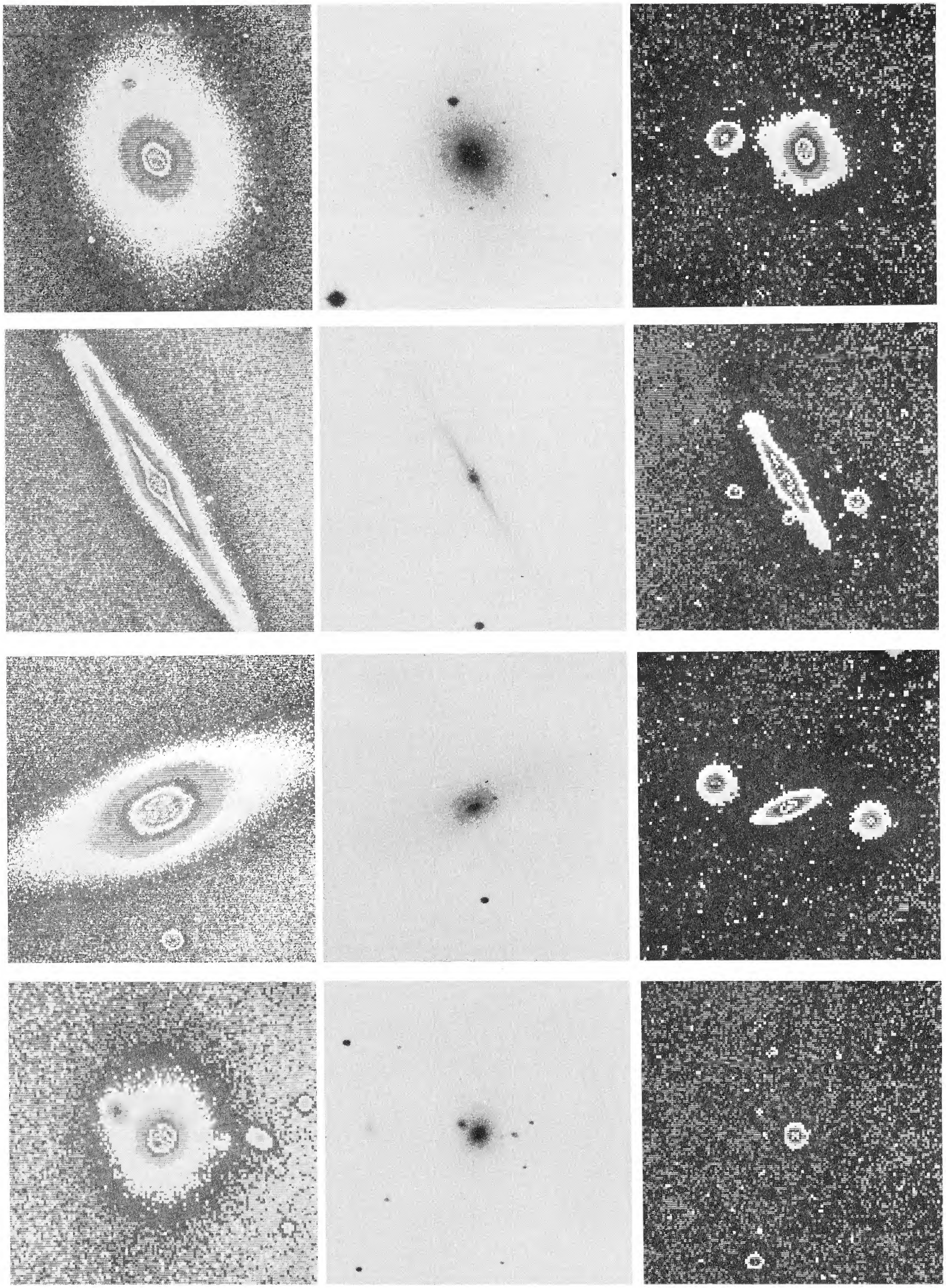

FIG. 2*a*

BURSTEIN (*see* page 438)

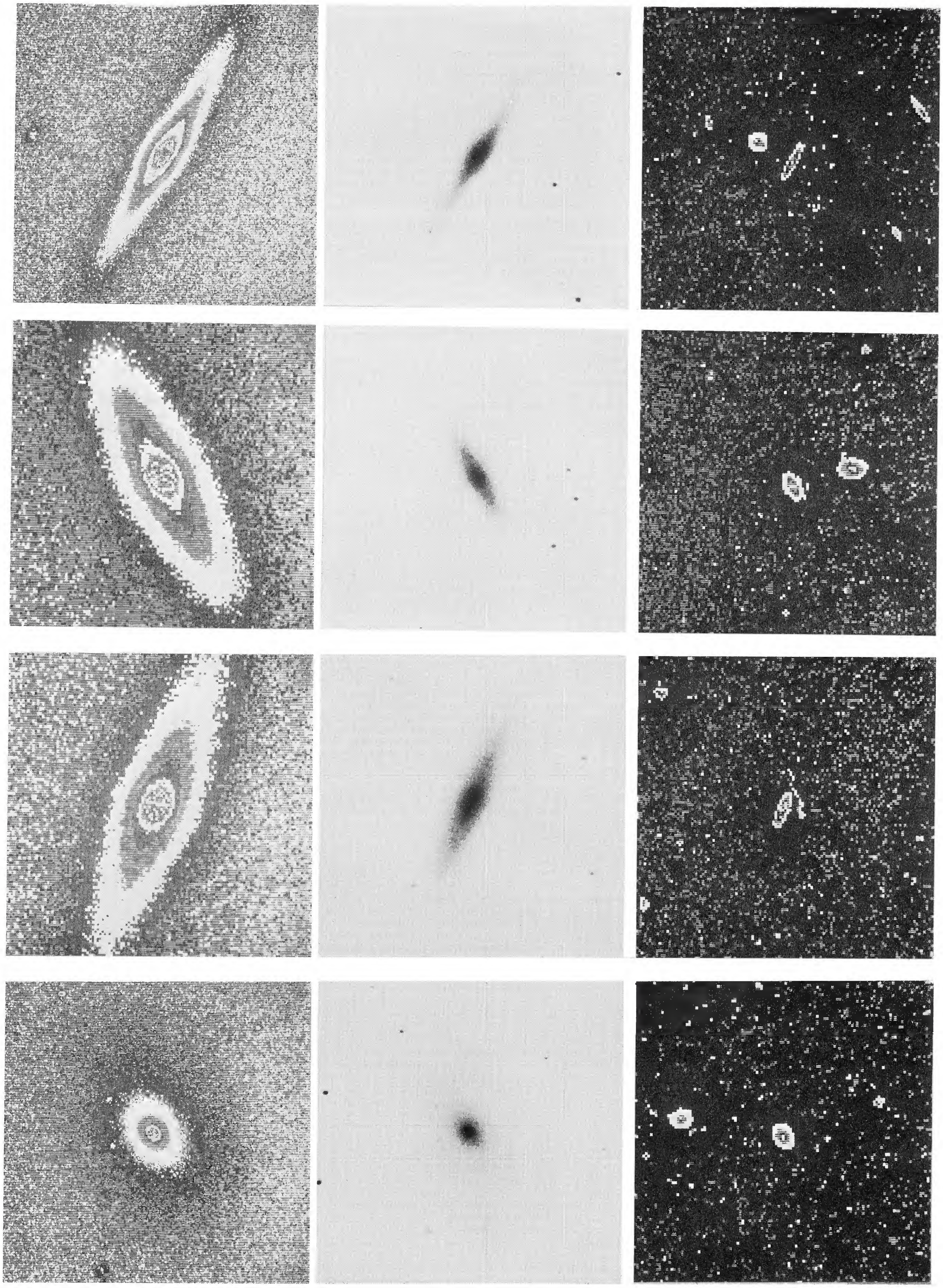

FIG. 2*b*

BURSTEIN (*see* page 438)

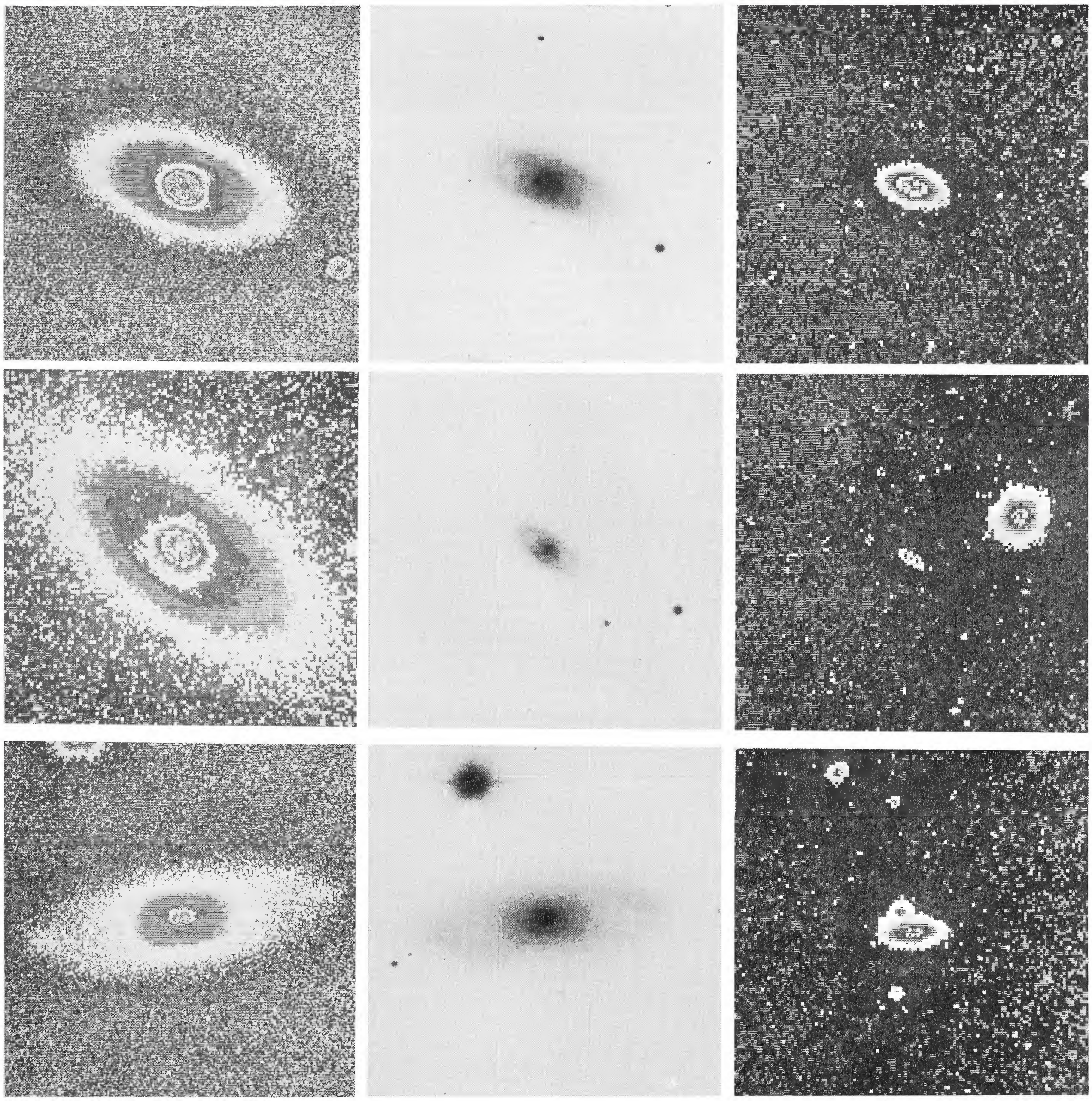

FIG. 2c

BURSTEIN (*see* page 438)

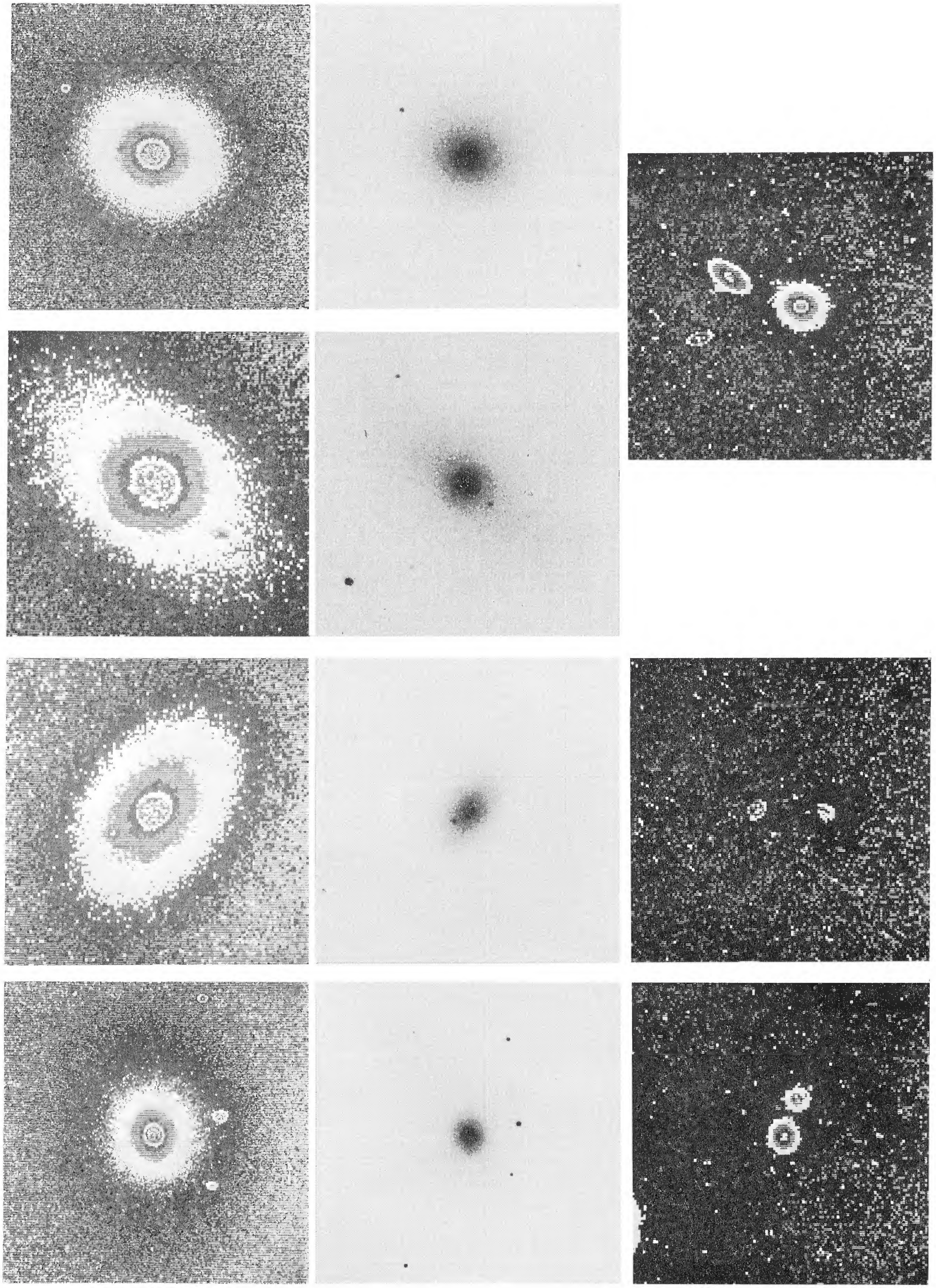

FIG. 2*d*

BURSTEIN (*see* page 438)

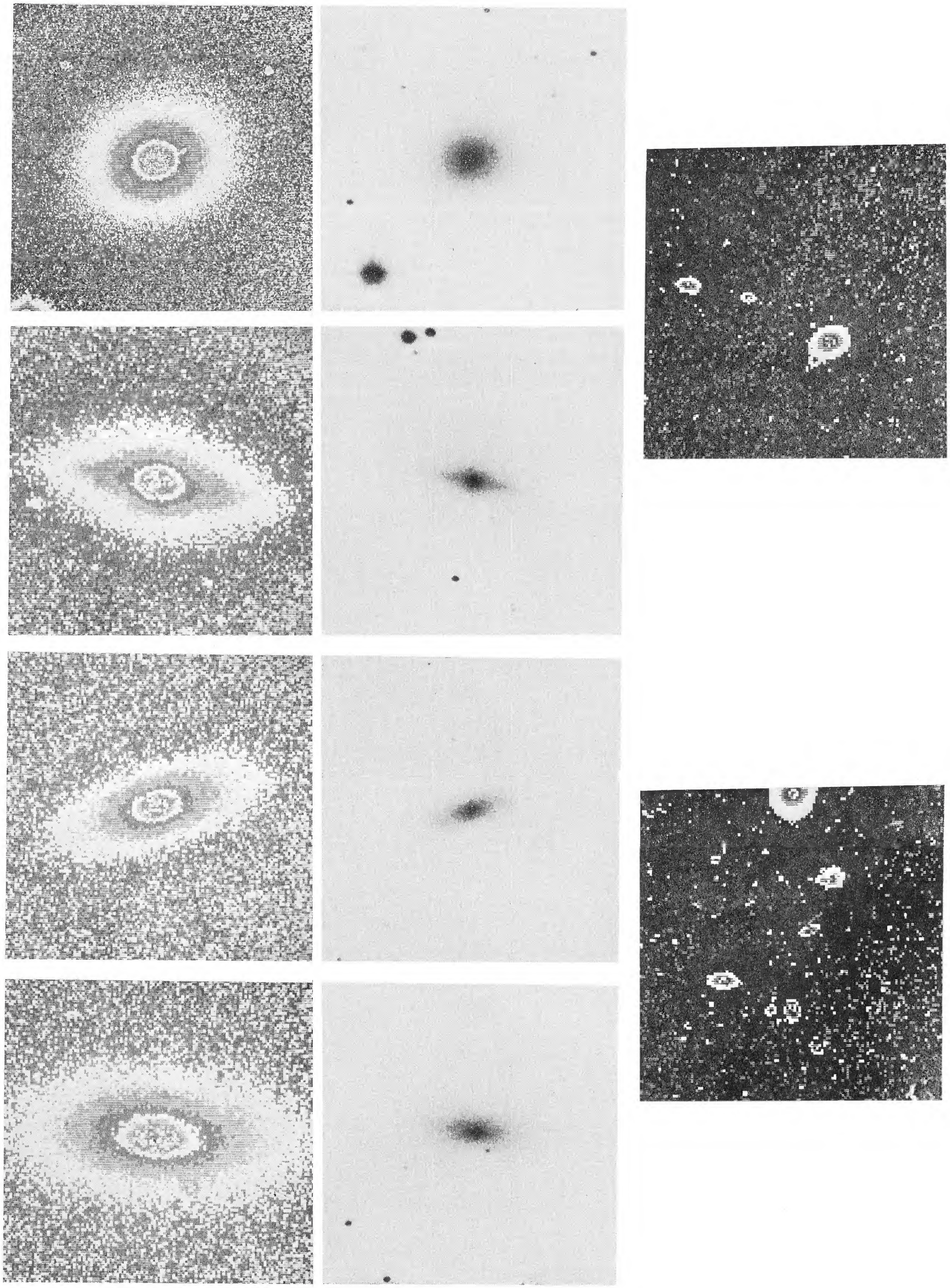

FIG. 2e

BURSTEIN (*see* page 438)

TABLE 2

Major- and Minor-Axis Luminosity Profiles

NGC 3379

PA = 60° (10° FROM MAJOR AXIS)

R	μ_B	R	μ_B
2	17.42	34	21.42
3	(17.89)	36	21.42
4	18.18	38	21.48
5	18.48	40	21.58
6	18.65	45	21.80
7	18.90	50	21.91
8	19.05	60	22.34
9	19.23	70	22.62
10	19.38	80	22.99
11	19.50	90	23.30
12	19.66	100	23.65
13	19.75	110	23.93
14	19.92	120	24.04
15	20.04	140	24.38
16	20.09	160	24.71
17	20.24	180	25.15
18	20.29	210	25.70
19	20.43	225	*25.85
20	20.45	255	*26.05
22	20.72		
24	20.85		
26	21.03		
28	21.06		
30	21.19		
32	21.30		

* = SW side only

NGC 3384

MAJOR AXIS				MINOR AXIS			
R	μ_B	R	μ_B	R	μ_B	R	μ_B
1	17.41	32	21.67	1	17.71	60	23.83
2	17.70	34	21.86	2	18.02	70	24.59
3	18.04	36	21.94	3	18.48	80	24.86
4	18.37	40	21.96	4	18.70	90	25.26
5	18.67	45	22.09	5	18.99	105	26.31:
6	18.93	50	22.23	6	19.33		
7	19.18	60	22.46	7	19.49		
8	19.41	70	22.65	8	19.66		
9	19.63	80	22.92	9	19.75		
10	19.83	90	23.14	10	19.90		
11	20.02	100	23.40	11	19.98		
12	20.09	110	23.65	12	20.19		
13	20.28	120	23.97	13	20.31		
14	20.48	130	24.32	14	20.36		
15	20.55	140	24.60	15	20.46		
16	20.68	150	25.17	16	20.63		
17	20.86	165	25.97	17	20.83		
18	20.88	180	26.17	18	21.03		
19	20.95			19	21.16		
20	21.04			20	21.39		
22	21.23			22	21.65		
24	21.36			24	21.82		
26	21.50			30	22.39		
28	21.55			40	22.87		
30	21.69			50	23.32		

NGC 3489

MAJOR AXIS				MINOR AXIS			
R	μ_B	R	μ_B	R	μ_B	R	μ_B
1	16.86	32	21.41	1	16.86	45	23.68
2	(17.09)	34	21.46	2	17.45	50	24.20
3	(17.55)	36	21.46	3	(17.96)	60	24.56
4	(18.16)	38	21.51	4	18.57	75	25.38
5	18.46	40	21.59	5	18.92	90	26.13
6	18.78	42	21.66	6	19.20		
7	18.85	45	21.80	7	19.46		
8	19.12	50	21.94	8	(19.60)		
9	19.21	60	22.55	9	(19.83)		
10	19.44	70	23.20	10	19.96		
11	19.66	80	23.66	11	20.11		
12	19.94	90	24.17	12	20.30		
13	20.11	100	24.57	13	20.45		
14	20.28	110	25.02	14	20.64		
15	20.39	120	25.23	15	20.74		
16	20.45	130	25.66	16	20.84		
17	20.57	140	26.09	17	20.99		
18	20.61			18	(21.09)		
19	20.60			19	21.24		
20	20.64			20	21.44		
22	(20.76)			22	21.60		
24	(20.84)			24	21.87		
26	21.10			26	22.17		
28	21.24			30	22.42		
30	21.32			40	22.92		

NGC 4111

MAJOR AXIS				MINOR AXIS	
R	μ_B	R	μ_B	R	μ_B
1	16.96	32	20.64	1	17.19
2	(17.12)	34	20.88	2	17.80
3	(17.42)	36	20.98	3	18.49
4	(17.67)	38	21.02	4	19.07
5	18.09	40	21.13	5	19.49
6	18.40	42	21.16	6	19.70
7	18.59	44	21.24	7	19.94
8	18.93	50	21.36	8	20.27
9	19.17	60	21.68	9	20.57
10	19.29	70	21.98	10	20.83
11	19.43	90	22.65	11	21.10
12	19.52	100	23.11	12	21.41
13	19.61	110	23.63	13	21.65
14	19.72	120	(24.16)	14	21.76
15	19.74	130	24.39	15	22.08
16	19.70	140	25.00	16	22.35
17	19.75	150	25.42	17	22.45
18	19.79			18	22.93
19	19.71			20	23.41
20	19.80			25	23.85
22	19.85			30	24.41
24	19.93			40	(25.20)
26	20.16			50	(25.70)
28	20.29			60	26.05
30	20.51				

NGC 4150

MAJOR AXIS				MINOR AXIS	
R	μ_B	R	μ_B	R	μ_B
0	17.64	30	22.32	0	17.64
1	18.05	32	22.44	1	18.19
2	(18.44)	34	22.72	2	(18.47)
3	(18.92)	40	23.19	3	19.08
4	19.45	45	23.52	4	19.66
5	19.86	50	24.06	5	20.16
6	20.19	60	24.21	6	20.46
7	20.39	75	26.14	7	20.70
8	20.55			8	20.97
9	20.72			9	21.21
10	20.77			10	21.32
11	20.90			11	21.50
12	21.15			12	21.52
13	21.19			13	21.70
14	21.28			14	21.81
15	21.36			16	22.00
16	21.44			18	22.27
17	21.54			20	22.48
18	21.63			24	22.96
19	21.70			30	23.66
20	21.73			40	24.67
22	21.84			50	25.41
24	21.95			60	25.82
26	22.16			70	26.06
28	22.20				

NGC 4203

MAJOR AXIS				MINOR AXIS			
R	μ_B	R	μ_B	R	μ_B	R	μ_B
0	17.79	30	22.04	0	17.79	60	23.24
1	18.01	40	22.47	1	(17.96)	70	23.84
2	18.32	50	22.75	2	18.26	80	24.11
3	18.68	60	23.02	3	18.54	90	24.65
4	18.91	70	23.41	4	18.95	100	25.21
5	19.25	80	23.71	5	19.28	110	25.64
6	19.48	90	*24.29	6	19.59	120	25.85
7	19.69	100	*24.78	7	19.80	130	26.03
8	19.87	110	*25.36	8	20.04		
9	20.02	120	*26.08	9	20.25		
10	20.13	130	*(26.70)	10	20.48		
11	20.26			11	20.59		
12	20.41			12	20.74		
13	20.52			13	20.87		
14	20.68			14	21.00		
15	20.78			15	21.15		
16	20.94			16	21.31		
17	21.05			17	21.42		
18	21.14			18	21.50		
19	21.37			19	21.51		
20	21.43			20	21.62		
22	21.57			25	21.82		
24	21.80			30	22.14		
26	21.86			40	22.51		
28	21.95			50	22.92		

* = SW side only

NGC 4270

MAJOR AXIS				MINOR AXIS	
R	μ_B	R	μ_B	R	μ_B
1	18.81	50	24.38	1	18.89
2	(19.00)	60	24.80	2	19.37
3	(19.35)	70	25.51	3	19.84
4	(18.71)	75	25.85	4	20.27
5	19.96			5	(20.70)
6	20.26			6	(20.98)
7	20.44			7	21.20
8	20.61			8	21.43
9	20.69			9	21.71
10	20.79			10	22.15
11	20.98			11	(22.27)
12	21.05			12	(22.39)
13	21.40			13	22.41
14	21.28			14	(22.76)
15	21.47			15	22.62
16	21.50			20	23.70
17	21.59			30	25.09
18	21.63			45	26.20
19	21.71				
20	21.78				
22	21.98				
24	(22.00)				
26	22.10				
30	22.32				
40	23.20				

NGC 4281

MAJOR AXIS				MINOR AXIS	
R	μ_B	R	μ_B	R	μ_B
0	17.88	30	21.81	0	17.88
1	18.01	35	22.07	1	(18.31)
2	18.46	40	22.46	2	(18.99)
3	18.78	50	22.99	3	(19.49)
4	19.17	60	23.33	4	(19.91)
5	19.35	70	23.92	5	20.17
6	19.70	80	24.34	6	20.36
7	19.92	90	24.75	7	20.61
8	20.09	100	25.10	8	20.85
9	20.21	110	25.40	9	21.05
10	20.39	120	26.03	10	21.27
11	20.57			11	(21.56)
12	20.63			12	21.67
13	20.71			13	21.70
14	20.74			14	21.90
15	20.81			15	22.00
16	20.85			16	22.19
17	20.99			17	22.18
18	21.04			18	22.41
19	21.30			19	22.49
20	21.10			20	(22.57)
22	21.32			25	23.06
24	21.41			30	23.44
26	21.59			40	24.27
28	21.70			50	24.83
				60	25.24
				70	25.67
				80	25.60
				90	26.04

TABLE 2—*Continued*

NGC 4324 — MAJOR AXIS

R	μ_B	R	μ_B
0	18.60	22	21.04
1	18.71		21.33
2	19.02	24	21.20
3	19.30		21.46
4	19.62		
5	19.83	26	21.51
6	20.08	28	21.78
7	20.20	30	21.85
8	20.40	35	22.28
9	20.55	40	22.52
10	20.68	50	23.14
11	20.75	60	23.61
12	20.96	70	23.90
13	20.96	80	24.29
14	21.09	90	24.73
15	21.18	100	25.20
16	21.19	110	25.80
17	21.21		
18	21.25		
19	21.20		
	21.32		
20	21.12		
	21.15		

NGC 4324 — MINOR AXIS

R	μ_B
0	18.60
1	18.76
2	19.13
3	19.48
4	19.83
5	20.11
6	20.31
7	(20.61)
8	(20.61)
9	20.75
10	20.79
11	21.09
12	21.28
13	21.47
14	21.66
15	21.77
16	22.10
17	22.81
18	22.95
20	23.23
25	23.51
30	23.86
40	24.97
45	25.41
50	26.10

NGC 4350 — MAJOR AXIS

R	μ_B	R	μ_B
0	17.34	30	20.95
1	17.50	35	21.40
2	(17.88)	40	21.68
3	18.55	45	22.11
4	18.69	50	22.31
5	18.98	60	22.94
6	19.23	70	23.66
7	19.35	80	24.26
8	19.46	90	24.84
9	19.51	100	25.27
10	19.65	105	25.58
11	19.71	120	25.80
12	19.81	135	26.32
13	19.83		
14	19.92		
15	19.91		
16	20.00		
17	20.09		
18	20.12		
19	20.16		
20	20.23		
22	20.36		
24	20.51		
26	20.64		
28	20.86		

NGC 4350 — MINOR AXIS

R	μ_B
0	17.34
1	17.52
2	18.24
3	18.67
4	19.06
5	19.53
6	19.86
7	20.17
8	20.53
9	20.86
10	21.07
11	21.38
12	21.62
13	21.76
14	21.99
15	22.25
20	22.90
25	23.34
30	23.56
40	24.16
45	24.32
50	24.55
60	24.80
70	25.20
75	25.45
105	26.20

NGC 4377 — MAJOR AXIS ONLY

R	μ_B
0	17.81
1	(18.13)
2	(18.52)
3	(18.99)
4	(19.41)
5	19.72
6	19.98
7	20.28
8	20.69
9	20.91
10	21.03
11	21.22
12	21.31
13	21.40
14	21.52
15	21.71
20	21.97
30	23.00
40	23.99
50	24.73
60	25.80

NGC 4382 — ALONG LINE TO NGC 4394

R	μ_B	R	μ_B
1	17.02	35	21.16
2	17.43	40	21.29
3	18.01	45	21.47
4	18.31	50	21.66
5	18.62	60	22.07
6	18.83	70	22.39
7	19.08	80	22.68
8	19.20	90	22.97
9	19.37	100	23.16
10	19.54	110	23.52
11	19.66	120	23.66
12	19.76	130	23.83
13	19.86	140	23.87
14	19.98	160	24.24
15	20.05	180	24.38
16	20.20	200	24.60
17	20.29	220	25.04
18	20.33	240	*25.21
19	20.39	260	*25.12
20	20.43	280	*25.62
22	20.47	300	*25.72
24	20.69	320	*25.52
26	20.83	340	*25.80
28	20.84		
30	21.01		

* = away from N 4394

NGC 4382 — PERPENDICULAR TO N4394 LINE

R	μ_B	R	μ_B
1	17.03	35	21.11
2	17.58	40	21.27
3	18.02	45	21.40
4	18.28	50	21.57
5	18.55	60	21.81
6	18.80	70	21.97
7	19.03	80	22.18
8	19.19	90	22.35
9	19.28	100	22.48
10	19.48	110	22.77
11	19.62	120	22.93
12	19.73	130	23.13
13	19.77	140	23.36
14	19.90	160	23.83
15	19.97	180	*(24.25)
16	20.09	200	24.66
17	20.21	220	24.77
18	20.28	240	25.17
19	20.35	260	25.42
20	20.42	280	25.73
22	20.54	300	(26.00)
24	20.63		
26	20.69		
28	20.80		
30	20.91		

* = SE side only

NGC 4429 — MAJOR AXIS

R	μ_B	R	μ_B	R	μ_B
1	18.71	16	20.90	170	25.12
2	18.88	17	20.97	180	25.43
3	19.19	18	20.98	190	25.56
4	(19.44)	19	21.09	200	25.94
5	(19.79)	20	21.17	210	(26.15)
6	(20.08)	22	21.29		
7	20.06	24	(21.44)		
	20.49	26	(21.43)		
		28	(21.54)		
8	20.27	30	21.86		
	20.45	35	22.05		
		40	22.18		
9	20.40	50	22.40		
	20.60	55	22.44		
10	20.51	60	22.48		
	20.71	70	22.48		
		80	22.57		
11	20.57	90	23.02		
	20.85	100	23.47		
12	20.67	110	23.84		
	20.77	120	24.12		
		130	24.39		
13	20.65	140	24.74		
14	20.75	150	24.83		
15	20.79	160	24.95		

NGC 4429 — MINOR AXIS

R	μ_B	R	μ_B
1	18.99	16	21.70
		17	21.51
2	19.10	18	21.32
	19.48	19	22.00
3	19.45	20	22.04
	20.05	25	22.39
		30	22.74
4	19.84	40	23.47
	20.50	50	23.96
5	20.03	60	24.32
	20.68	70	*24.81
		80	*25.07
6	20.11	90	*25.44
	20.54	100	*25.56
7	20.35	105	*26.00
	20.52		
8	20.58		
9	20.61		
10	20.85		
11	21.00		
12	21.16		
13	21.35		
14	21.37		
15	21.62		

* = SW side only

NGC 4459 — MAJOR AXIS

R	μ_B	R	μ_B
0	17.20	19	21.06
		20	21.10
1	17.23	22	21.28
	17.87	24	21.43
2	18.13	26	21.55
	18.40	28	21.64
		30	21.81
3	18.62	35	22.08
	18.91	40	22.36
4	19.17	50	22.82
5	19.50	60	23.24
6	19.73	70	23.51
7	19.83	80	23.77
8	19.98	90	24.03
9	20.00	100	24.34
10	20.12	110	24.77
11	20.25	120	24.90
12	20.30	130	25.07
13	20.48	140	25.62
14	20.61	160	25.92
15	20.65		
16	20.76		
17	20.90		
18	20.98		

NGC 4459 — MINOR AXIS

R	μ_B	R	μ_B
0	17.20	15	20.96
		16	21.02
1	17.82	17	21.21
	17.39	18	21.30
2	18.80	19	21.43
	17.86	20	21.52
		22	21.62
3	19.20	24	21.89
	18.73	26	21.92
4	19.63	28	22.04
	19.00	30	22.25
		35	22.54
5	20.01	40	22.87
	19.31	50	23.36
6	19.92	60	23.73
	19.63	70	24.24
		80	24.32
7	19.91	90	24.76
8	19.96	100	*25.20
9	20.12	120	*26.05
10	20.24		
11	20.50		
12	20.66		
13	20.65		
14	20.77		

* = SW side only

TABLE 2—*Continued*

NGC 4474

MAJOR AXIS				MINOR AXIS	
R	μ_B	R	μ_B	R	μ_B
1	18.60	35	22.34	1	18.64
2	18.90	40	22.72	2	18.99
3	19.16	50	23.40	3	19.46
4	19.51	60	24.23	4	19.88
5	19.84	70	24.99	5	20.29
6	20.03	80	(25.40)	6	20.59
7	20.23	105	26.35	7	20.85
8	20.43			8	21.12
9	20.60			9	21.44
10	20.73			10	21.71
11	20.84			11	21.98
12	20.81			12	21.96
13	20.89			13	22.09
14	20.90			14	22.15
15	21.00			16	22.49
16	21.13			18	22.64
17	21.11			20	22.86
18	21.15			24	23.29
19	21.33			30	23.76
20	21.26			40	24.35
24	21.45			50	25.07
28	21.90			60	25.44
30	21.95			70	25.94

NGC 4526

MAJOR AXIS				MINOR AXIS			
R	μ_B	R	μ_B	R	μ_B	R	μ_B
1	17.50	30	20.80	1	18.26	19	20.90
2	17.93	35	21.04		17.10	20	20.99
3	18.15	40	21.30	2	18.72	22	21.08
4	18.37	50	21.52		17.64	24	21.43
5	18.63	60	21.67	3	19.15	30	21.95
6	+18.91	70	21.90		18.50	40	22.80
7	+19.20	80	22.06	4	19.05	50	23.48
8	+19.49	90	22.25		18.79	60	24.03
9	+19.68	100	22.45	5	19.03	70	24.47
10	+19.74	110	22.64	6	19.19	80	24.78
11	+19.91	120	22.90	7	19.40	90	24.97
12	+19.94	130	23.09	8	19.51	100	25.32
13	+19.95	140	*23.30	9	19.66	120	*25.76
14	+19.97	160	*23.91	10	19.82	* = NE side only	
15	+19.98	180	*24.11	11	19.99		
16	+19.95	200	*24.49	12	20.13		
17	+19.94	220	*24.84	13	20.29		
18	+20.12	240	*25.28	14	20.36		
19	+20.25	260	*25.66	15	20.47		
20	+20.25	280	*25.85	16	20.56		
22	+20.43	300	*26.00	17	20.69		
24	20.53	320	*26.20	18	20.83		
26	20.59	* = NW side only					
28	20.74	+ = SE side only					

NGC 4570

MAJOR AXIS				MINOR AXIS	
R	μ_B	R	μ_B	R	μ_B
1	(17.70)	35	21.41	1	17.59
2	(18.26)	40	21.56	2	18.21
3	(18.60)	50	21.95	3	18.77
4	18.84	60	22.36	4	19.19
5	18.98	70	22.74	5	19.64
6	19.23	80	23.35	6	19.96
7	19.59	90	23.71	7	20.30
8	19.65	100	24.47	8	20.57
9	19.84	110	24.94	9	20.91
10	19.88	120	25.40	10	21.20
11	19.99	140	26.02	11	21.35
12	20.04			12	21.65
13	20.08			13	21.86
14	20.14			14	22.07
15	20.20			20	23.35
16	20.27			25	23.98
17	20.41			30	24.31
18	20.46			45	25.43
19	20.37			60	26.07
20	20.55				
22	20.72				
24	20.94				
26	20.94				
28	21.03				
30	21.16				

NGC 4578

MAJOR AXIS				MINOR AXIS	
R	μ_B	R	μ_B	R	μ_B
0	18.14	60	23.69	0	18.14
1	18.58	70	*24.08	1	18.56
2	18.85	80	*24.57	2	18.94
3	19.24	90	*25.17	3	19.38
4	19.55	100	*25.47	4	19.77
5	19.79	110	*25.87	5	20.12
6	20.05	120	*26.30	6	20.48
7	20.29			7	20.75
8	20.47			8	20.98
9	20.69	* = SW side only		9	21.06
10	20.81			10	21.26
11	21.03			11	21.49
12	21.13			12	21.67
13	21.32			13	21.82
14	21.35			14	21.84
15	21.55			15	21.94
16	21.58			16	22.05
17	21.60			17	22.13
18	21.80			18	22.22
19	21.90			20	22.41
20	21.94			25	22.82
25	22.21			30	23.14
30	22.56			40	23.65
40	23.08			50	24.14
50	23.42			60	24.64
				70	25.1[illegible]
				80	25.80

NGC 4762

MAJOR AXIS				MINOR AXIS	
R	μ_B	R	μ_B	R	μ_B
1	17.82	38	20.05	1	18.00
2	18.23	40	20.09	2	18.40
3	18.69	45	20.31	3	18.84
4	18.82	50	20.51	4	19.10
5	19.08	55	20.73	5	19.51
6	19.17	60	20.86	6	19.78
7	19.39	65	21.00	7	20.12
8	19.49	70	21.06	8	20.39
9	19.52	75	21.10	9	20.65
10	19.52	80	21.14	10	20.90
11	19.59	90	21.21	12	21.35
12	19.70	100	21.59	14	21.74
13	19.64	110	(22.12)	16	22.00
14	19.68	120	22.77	18	22.25
15	19.74	130	23.08	20	22.52
16	19.74	140	23.24	25	23.07
17	19.72	150	23.32	30	23.23
18	19.77	160	23.31	40	23.95
19	19.80	180	23.56	50	24.62
20	19.79	200	23.77	60	*24.95
22	19.78	220	24.01	70	*25.80
24	19.79	240	24.32	80	26.05
26	19.81	260	25.32		
28	19.86		24.24	* = NE side only	
30	19.87				
32	19.92	280	25.80		
34	19.95		26.25		
36	20.00				

NOTE.—The luminosity profiles are listed as radius (in arcsec) and μ_B for the major axis of each program S0 galaxy and for the minor axes of all program galaxies except NGC 4377. The profiles, as listed, are the average of the two halves of the major- or minor-axis, Crossley plus Palomar data, with the following exceptions: (*a*) If a star is superposed on one side of a major or minor axis, only the data from the opposite side are used in the area affected (refer to Fig. 1 and the notes to Table 1 for these galaxies). (*b*) If the two sides of the profile disagree by more than 0.1 μ and if that disagreement is likely to be due to a real difference (e.g., presence of a dust lane) between the two sides of the profile, then the luminosity profiles of both sides of the galaxy are given. (*c*) If a luminosity profile of a neighboring star (or galaxy in the cases of NGC 3379 and 4382) is superposed on one part of a major or minor axis, the luminosity profile of the opposite side of that axis is given and is noted with an asterisk.

the present data and those of others are presented in graphical form in Figure 3 as deviations $\Delta\mu_B$ [$= \mu_B$ (Burstein) $- \mu_B$(other)] or as μ_B(Burstein) $- \mu_G$(Kormendy) along the major-axis profile, as well as sometimes along the minor-axis profile.

The comparisons made in Figure 3 are with the data of Burkhead and Kalinowski (1974, referred to in Fig. 3 as BK), King (1978), Kormendy (1977, KORM),[2] van Houten (1961, vH), Markarian, Oganesian, and Arakelian (1964, MOA), Tsikoudi

[2] The profile for NGC 3379 given in this paper is for P.A. = 60°, while the major-axis profile is near P.A. = 70°. However, since NGC 3379 has $b/a = 0.9$ (i.e., it is an E1 galaxy), the angle difference of 10° corresponds to a scale difference of only 0.15%. Thus the P.A. difference has a negligible effect on the comparisons in Fig. 3*a*.

(1977, Tsi), Benedict (1971, GFB), and Fraser (1977, F). The galaxies common to each study are given in the figure; note also the different vertical scales on the various graphs.

The comparisons in Figure 3 represent three apparent levels of agreement (neglecting zero-point differences): Level 1, $\Delta\mu < 0.05\,\mu$ from 18.5 to 25 μ; no obvious large ($> 0.1\,\mu$) systematic differences between the present data and those of Burkhead and Kalinowski, King, and Kormendy. Level 2, $\Delta\mu \approx 0.1$–$0.2\,\mu$ on average; systematic differences up to 0.5 μ at worst between the present data and the data of van Houten, Markarian *et al.*, and Tsikoudi and the data of Liller at $\mu_B > 21\,\mu$. Level 3, $\Delta\mu > 0.4\,\mu$; large systematic differences between our data and the data of Fraser (1977) and Benedict (1971) and the data of Liller at $\mu_B < 21\,\mu$.

It is unlikely that the large discrepancies in Figure 3 are due to errors in the present data (cf. Burstein 1978). For example, the disagreement here with Fraser is the worst shown in Figure 3; two facts argue strongly that this difference is due to large systematic errors in Fraser's data: (1) Three of the galaxies in common with Fraser (NGC 4762, 4459, and 4526) are also in common with at least one other observer, and the comparisons with the other observers do not exhibit as large a discrepancy as the comparison with Fraser (especially NGC 4459 in Fig. 3*a*). (2) Comparison of the nine galaxies in common with King (1978) and Fraser shows that the data for six galaxies disagree in the same manner (zero-point differences ignored) as do the data for four of the five galaxies in Fig. 3*f*.

The most reliable data in these comparisons are the photoelectric observations of Burkhead and Kalinowski (1974; see the comparison of their data with those of Miller and Prendergast 1962), which agree well with the present results as do the data of King and of Kormendy. Furthermore, the external errors of the present observations, as evidenced by the agreement with the observers in the level 1 category, are the same as the internal errors obtained by intercomparing the Crossley and the Palomar data. Thus one concludes that the intercomparison of the Crossley and the Palomar data is probably a valid estimate of the external errors in the present surface photometry data and that the real accuracy of the present data is best reflected in the comparisons in the level 1 category.

V. S0 LUMINOSITY PROFILES

a) Observed Light Distributions in S0 Galaxies

Each of the observed physical components of a galaxy appears to have its own identifying luminosity profile. The luminosity profile of an elliptical, or a bulge of an S0 or spiral, usually follows a de Vaucouleurs $R^{1/4}$ law (de Vaucouleurs 1959) (or a Hubble or King law [Kormendy 1976]). The profile of a disk is most often approximately exponential ($I = I_0 e^{-\alpha r}$ [Freeman 1970]), as are also possibly lenses (Kormendy 1977); bars or rings identify themselves by their distinctive two-dimensional appearance. Therefore, in principle one could identify the various dynamical components of a galaxy by analyzing only the luminosity profile.

Freeman (1970) used this property of luminosity profiles to model the structure of disks in terms of an exponential light distribution (de Vaucouleurs 1959). Freeman divided disks into two types. In Type I disks, the light distribution along the major axis is exponential and the bulge light distribution merges smoothly with that of the disk. Type II disks have light distributions that are not exactly exponential but have a change in the slope of the disk profile somewhere outside the bulge. (NGC 7457, in Kormendy 1977, is a good example of a Type I disk; NGC 4111 in Fig. 1 is an example of a Type II disk.)

Freeman found that both S0's and spirals had Type II disks, which were interpreted as perhaps being physically different from Type I disks. However, all but one of the Type II S0's in Freeman's sample came from the photometry of Liller (1960, 1966), and the Type II classification of these S0's was in large part due to the errors in her data (cf. also the discussion in Kormendy 1977).

Inspection of the (μ_B, r) profiles in Figure 1 shows that almost all of the S0 disks in the present sample have luminosity profiles that can be approximated by an exponential, but that few disks can be said to be exactly exponential. The great variety of disk luminosity profiles are too complex to be described by the simple Type I–Type II classification. There appears to be a continuum of disk profile types which appear in a (μ_B, r)-plot as variations of a profile from an exact exponential. These variations seem to be similar in shape—instead of a straight line in a (μ_B, r)-plot, the

FIG. 1.—Major- and minor-axis luminosity profiles for the 18 program S0 galaxies plotted as μ_B (blue magnitudes arcsec^{-2}) versus r (radius, in arcsec). *Small squares and small pluses*, Crossley inner data, interpolated to every 1″; *small diamonds and small crosses*, Palomar inner data, interpolated to every 2″. *Pluses and crosses* refer to the same side of the major (minor) axis; *squares and diamonds* refer to the other side. Large symbols are from the outer scans and correspond to the same sides of the galaxy as their small-symbol counterparts; Crossley outer data are interpolated to every 10″; Palomar outer data are interpolated to every 15″. Stars influencing the light distribution of a profile are marked with an *S*, dust lanes with a *D*, and plate defects with an *F*. (*a*) NGC 3384, 3489, 4350, and 4111; (*b*) NGC 4281, 4270, 4150, and 4459 (note the two scales on the ordinate: the lower scale applies to NGC 4459, the upper scale to the other three galaxies); (*c*) NGC 4578, 4474, 4324, and the major axis only of NGC 4377; (*d*) NGC 4203, 4429, and 4570; (*e*) NGC 4762, 4526, and 4382. Intervals of $\mu_B = 1.0\,\mu$ are marked on the abscissa, with the zero point in μ_B for each profile noted.

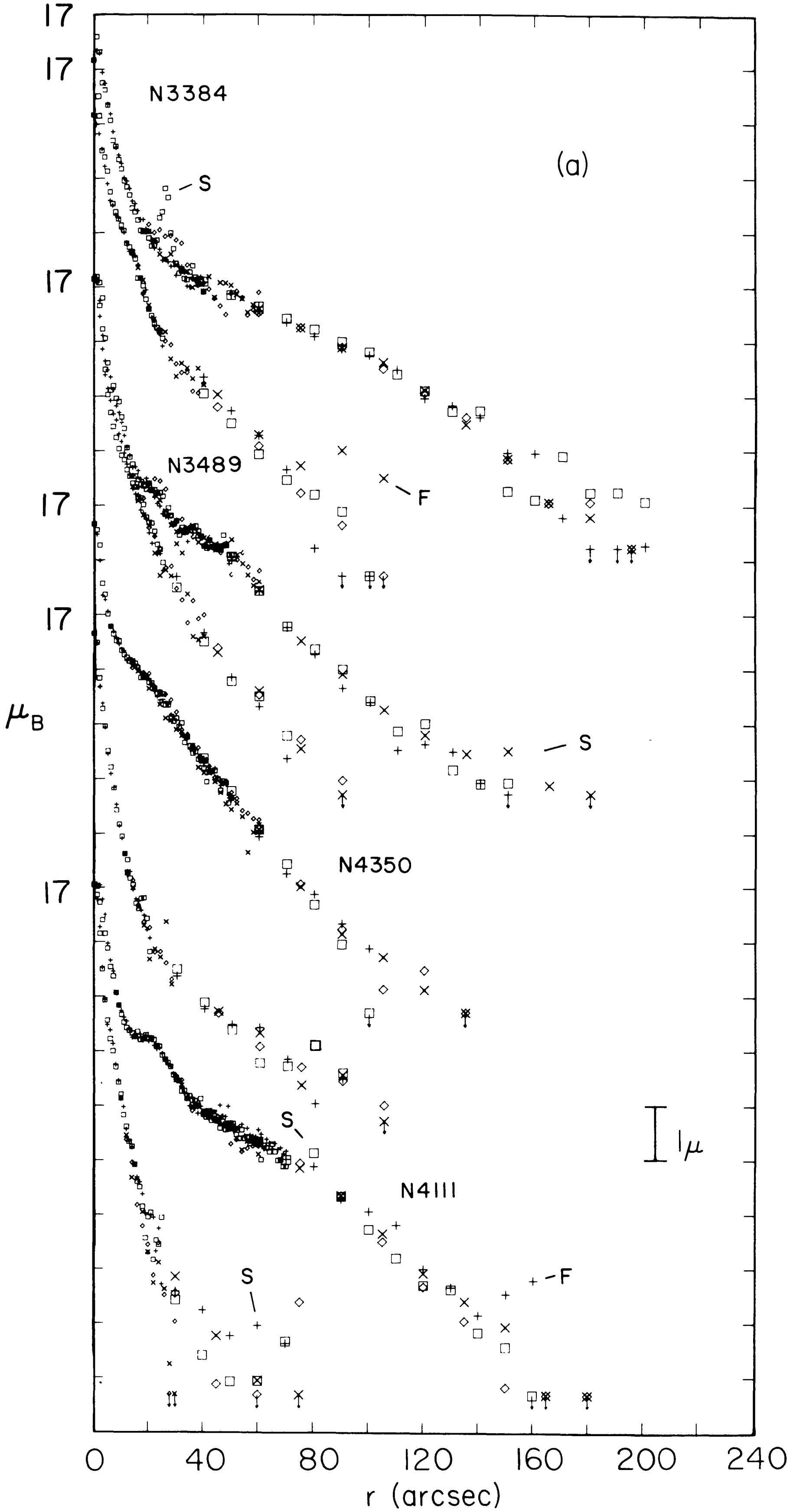
17
17
17
17
17
17
N3384
(a)
S
N3489
F
μ_B
S
N4350
S
N4111
F
1μ
0
40
80
120
160
200
240
r (arcsec)

FIG. 1*a*

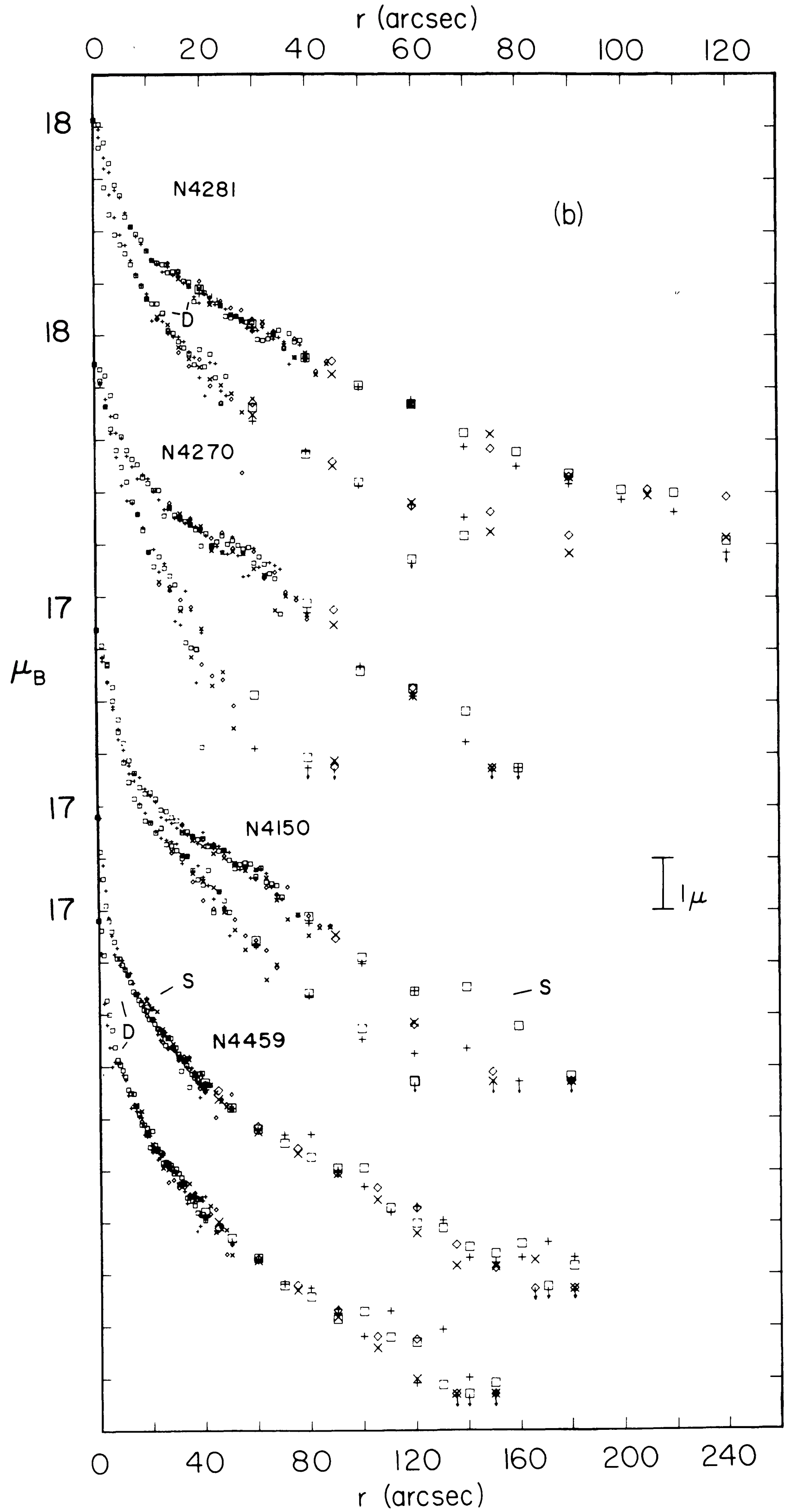
r (arcsec)
0
20
40
60
80
100
120
18
N4281
(b)
18
D
N4270
17
μ_B
17
N4150
17
1μ
S
S
D
N4459
0
40
80
120
160
200
240
r (arcsec)

FIG. 1b

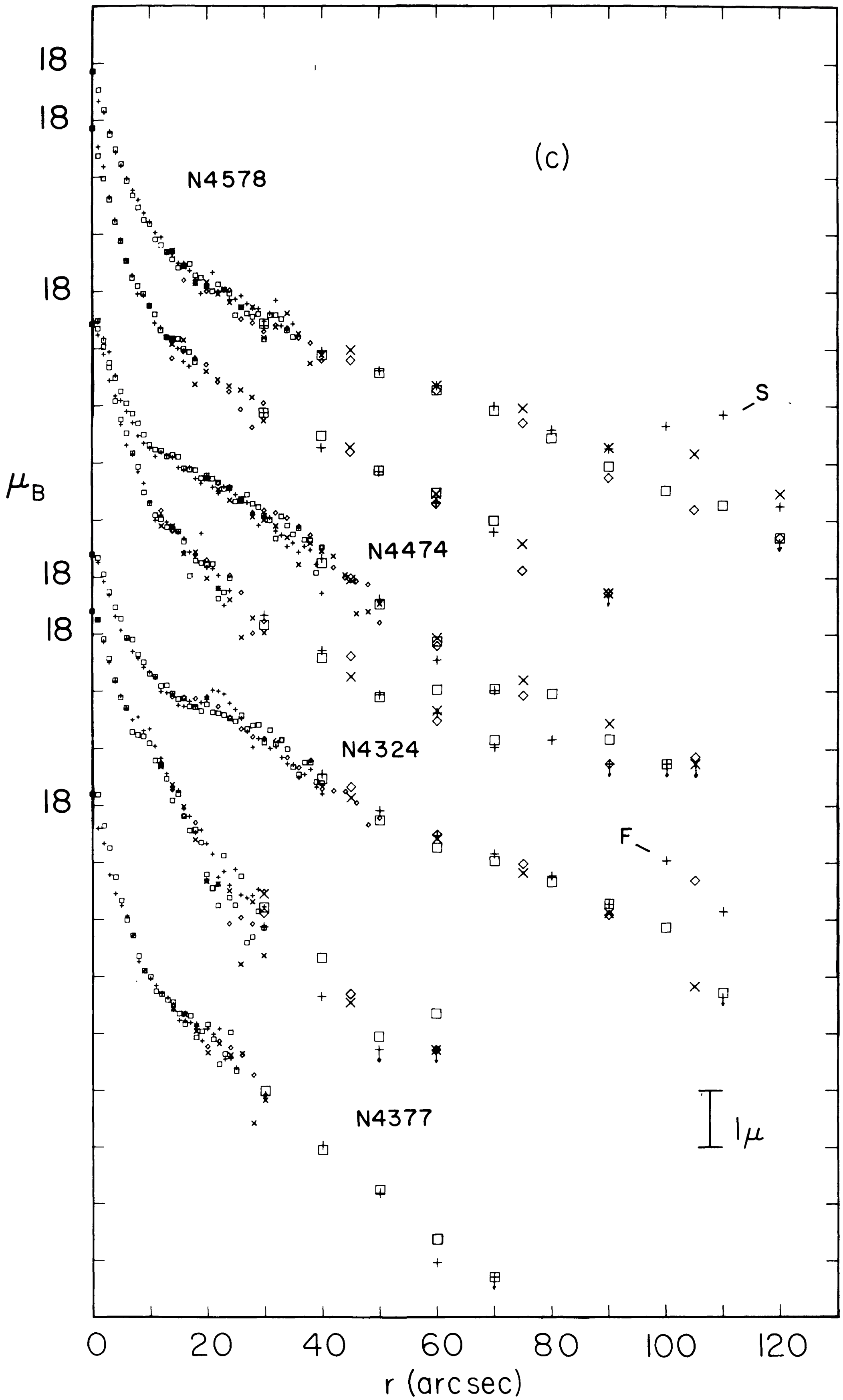

18
18
18
18
18
18
μ_B
(c)
N4578
N4474
N4324
N4377
S
F
1μ
0
20
40
60
80
100
120
r (arcsec)

FIG. 1c

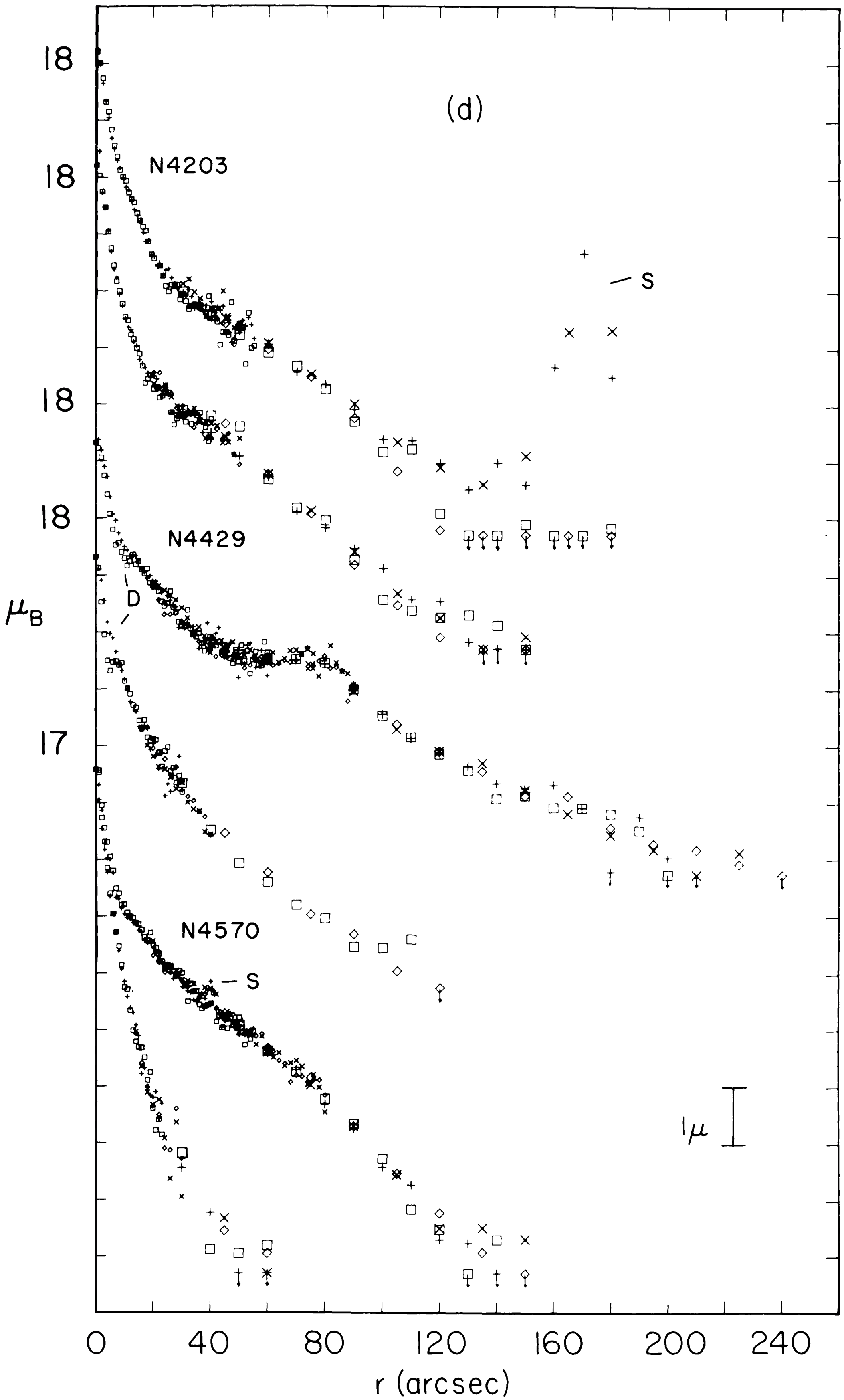

18
18
18
18
17
(d)
N4203
N4429
N4570
S
D
S
μ_B
1μ
0
40
80
120
160
200
240
r (arcsec)

FIG. 1*d*

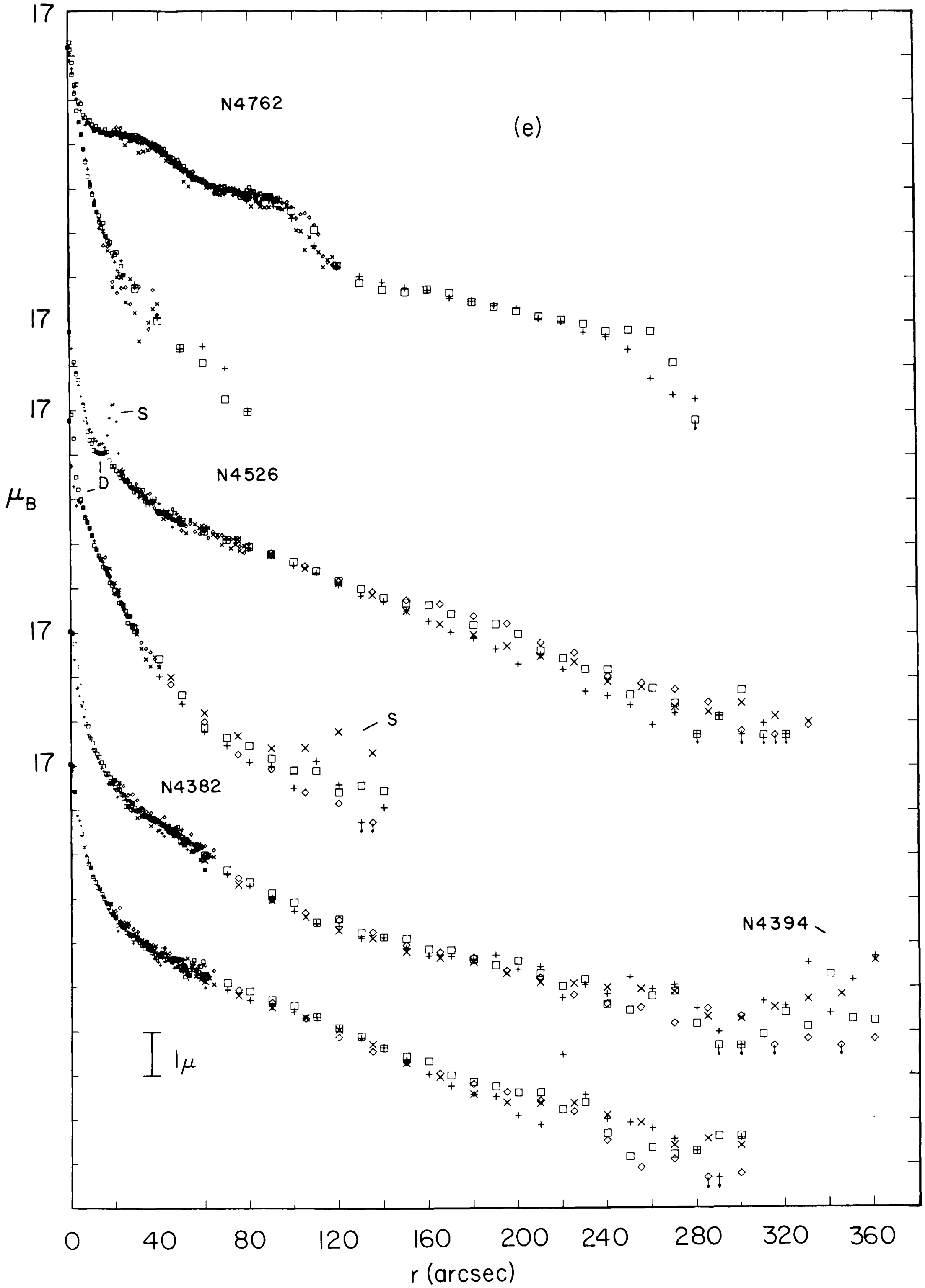

17
17
17
17
17
N4762
(e)
S
D
N4526
μ_B
S
N4382
N4394
1μ
0
40
80
120
160
200
240
280
320
360
r (arcsec)

FIG. 1e

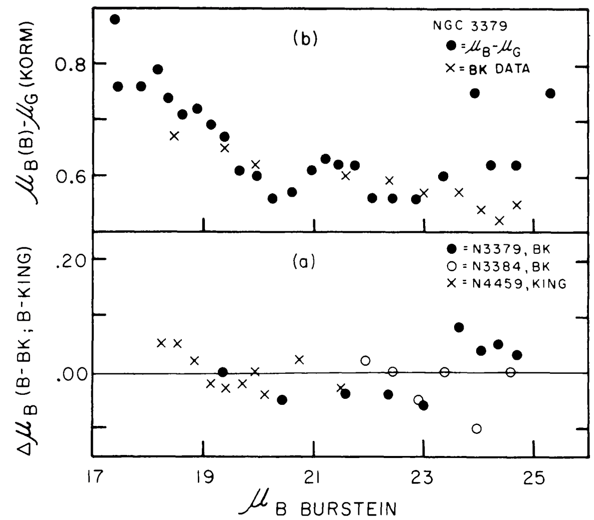

FIG. 3.—Comparisons of the present surface photometry with that of others plotted (for the major axis only unless otherwise noted) as differences, in magnitudes, versus μ_B(Burstein). (*a*) Comparison with the data of Burkhead and Kalinowski (1974, BK) for (*filled circles*) NGC 3379 and (*open circles*) NGC 3384, and with the data of King (1978) for (*crosses*) NGC 4459; $\Delta\mu_B$(B − BK) or $\Delta\mu_B$(B − King) < 0.05 μ (see also n. 2 of the text). (*b*) Comparison with the data of Kormendy (1977, KORM) for NGC 3379 (see also n. 2 of the text). Since Kormendy's data are given in μ_G, not μ_B, the difference μ_B(B) − μ_G(KORM) is plotted as filled circles. The photoelectric color gradient $\mu_B - \mu_G$, as determined from the data of Burkhead and Kalinowski and the *B* to *G* transformation given in Kormendy (1977), is plotted as crosses. The scatter of μ_B(B) − μ_G(KORM) < 0.05 μ. (*c*) Comparison with the data of van Houten (1961, vH) and Markarian Oganesian, and Arakelian (1964, MOA); galaxies and major and minor axes compared are as noted in the figure (NGC 4459 only, from Markarian *et al.*). (*d*) Comparison with the data of Liller (1960, 1966, L) for eight galaxies. (*e*) Comparison with the data of Tsikoudi (1977, Tsi) and of Benedict (1971, GFB). (*f*) Comparison with the data of Fraser (1977, F).

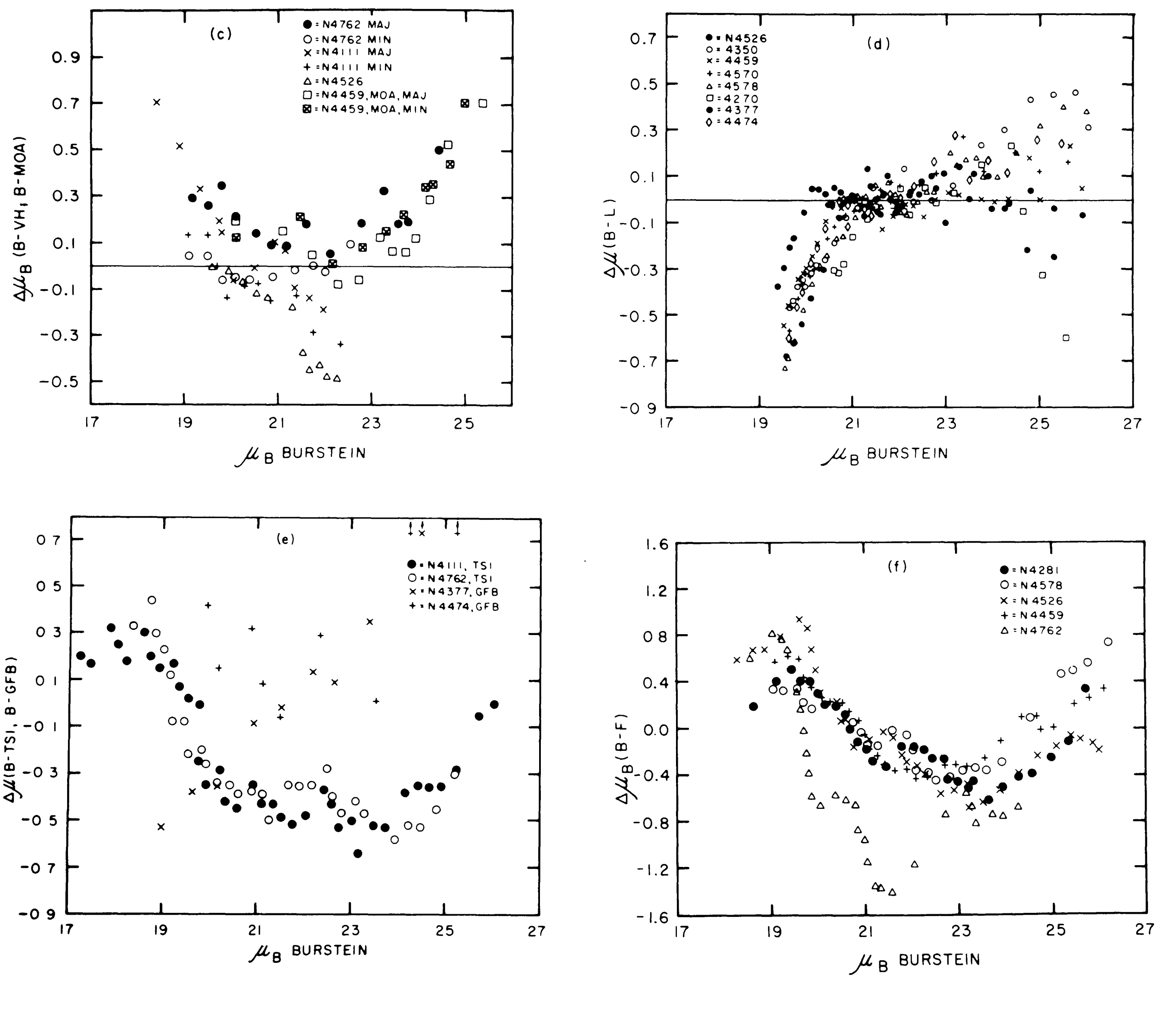

profile is curved downward and the radial scale of the curvature and the amplitude of the curve can vary. The exponential disk can be gently curved for most of the length of the disk (as in NGC 3384, in the outer disk of NGC 4111, or in NGC 4474); or the disk can be nearly exponential over much of the galaxy, with a small scale curvature in the profile, usually near the center (e.g., NGC 4350, 4570). The amplitude of both the large- and the small-scale curvatures can vary in size, from the large-amplitude lens/bar portions of NGC 4111, 4429, and 4762 to the barely perceptible change in curvature in NGC 4570. A disk can also have more than one variation on similar or different scales (e.g., NGC 4111).

As pointed out by Kormendy (1977), different physical components may have the same type of luminosity profile. If this is true, the interpretation of disk luminosity profiles is not straightforward, and the variations among disks can arise from a number of different effects, including real dynamical differences among different parts of a disk profile. Further work on the classification of disk profiles is needed, especially in determining how the variations in disk profiles correlate with other properties of the galaxy (e.g., the presence of neighbors or $\mathscr{D}/\mathscr{B}$).

b) Peculiar S0's

By the way the S0 class is defined, S0's are usually thought to have relatively featureless disks in comparison to spirals. Most of the S0's in the present program were chosen because of their apparent "normality," as evidenced by information available at the time. Thus it was somewhat surprising to find that a significant fraction of these S0's were peculiar in one way or another.

Of the 18 S0's in this sample, only one—NGC 4382—was classified as peculiar in the *Reference Catalogue of Bright Galaxies* (de Vaucouleurs and de Vaucouleurs 1964) (NGC 4474, as seen in Table 1, is also classified as peculiar in the *Second Reference Catalogue of Bright Galaxies* [de Vaucouleurs, de Vaucouleurs, and Corwin 1976, RCBG II]). NGC 4762 was also included in this investigation because of its extreme thinness, even though it violates condition (iii) of § II (it probably has a strong bar; cf. the plate in the *Hubble Atlas of Galaxies* [Sandage 1961] and RCBG II classification).

Of the remaining 16 S0's, five—NGC 3489, 4270, 4324, 4429, and 4526—have noticeable departures from symmetry in their disk or bulge structure. NGC 4324 has been detected in 21 cm neutral hydrogen (Krumm and Salpeter 1976) and has been roughly mapped in 21 cm (Krumm 1977). As seen in the isophotal picture of Figure 2, the "ring" in this galaxy is not complete but has a gap on the southwest side of the major axis. In addition, the Crossley plates show weak structure in the "ring." One explanation of NGC 4324 is that this "ring" is not a true ring, but rather a tightly wound spiral arm (or arms), and the galaxy is a misclassified spiral or S0/a. Because of this, NGC 4324 will be excluded from further discussion.

NGC 4526 has been classified as an SAB0 (RCBG II), which means that it was thought to have a weak bar. The barlike structure in NGC 4526, which is centered at $r = 35''$–$40''$, is shown in Figure 4 (Plate 28), taken from a Crossley Kodak 103a-D + Schott GG 14 plate (photographic "V"). As one can see, this "bar" is really made up of small spiral-type distortions. These spiral-type distortions appear more clearly on a V plate than on a B plate, implying that they are at least as red as the rest of the galaxy. No 21 cm neutral hydrogen emission has been detected in NGC 4526.

The brightness distribution of NGC 4429, as seen in the isophotal picture of Figure 2 is not axially symmetric but is more like a much subdued spiral pattern. It is likely that the "ring" in NGC 4429 is also comprised of tightly wound spiral arms; but these arms are broad and smooth compared with those in NGC 4324, consistent with the fact that no 21 cm neutral hydrogen emission has yet been detected in NGC 4429.

A careful examination of isophotal maps of NGC 4270 turned up evidence for a slight spiral-like distortion in its disk. This was confirmed on a long-exposure IIIa-J Schmidt plate of this galaxy taken by Kormendy (1977, private communication) which shows this slight distortion becoming a large warp in the luminosity distribution at very faint light levels. Since this galaxy has several near neighbors, this structure may be tidal in origin.

NGC 3489 has a very unusual bulge light distribution, as seen in the isophotal picture in Figure 2; the bulge is boxlike rather than elliptical. This might be an example of a galaxy like NGC 128 (Sandage 1961) seen more face-on, but NGC 3489 has no obvious near neighbors.

As seen in Figure 2, NGC 4382 is contained in a common envelope with its companion, NGC 4394. It is evident from both the high- and low-resolution isophotal pictures that the S0 is tidally distorted by its smaller companion. The position of the major axis in NGC 4382 rotates with increasing distance from its center (also noted by King 1978) until some of the outermost isophotes become diamond shaped, with one edge touching NGC 4394. The line-of-sight velocity difference between the two galaxies is essentially zero; thus these objects may form a bound double galaxy. Kormendy (1976), in his analysis of possible tidal effects on the luminosity profiles of elliptical galaxies, inferred from the luminosity profile of NGC 4382 (taken from King 1978) that this galaxy was likely to be tidally distorted.

The primary type of peculiarities found in these S0's are the result of either tidal interactions (NGC 4382), spiral-type distortions (NGC 4324, 4429, 4526), or a combination of the two effects (NGC 4270). The selection bias in this sample of S0's was to select against S0's with obvious peculiar disk characteristics. Since four of the 16 "normal" S0's do exhibit subtle nonaxisymmetric phenomena in their disks, it would appear that there may exist as many "peculiar" S0's as there are "normal" S0's.

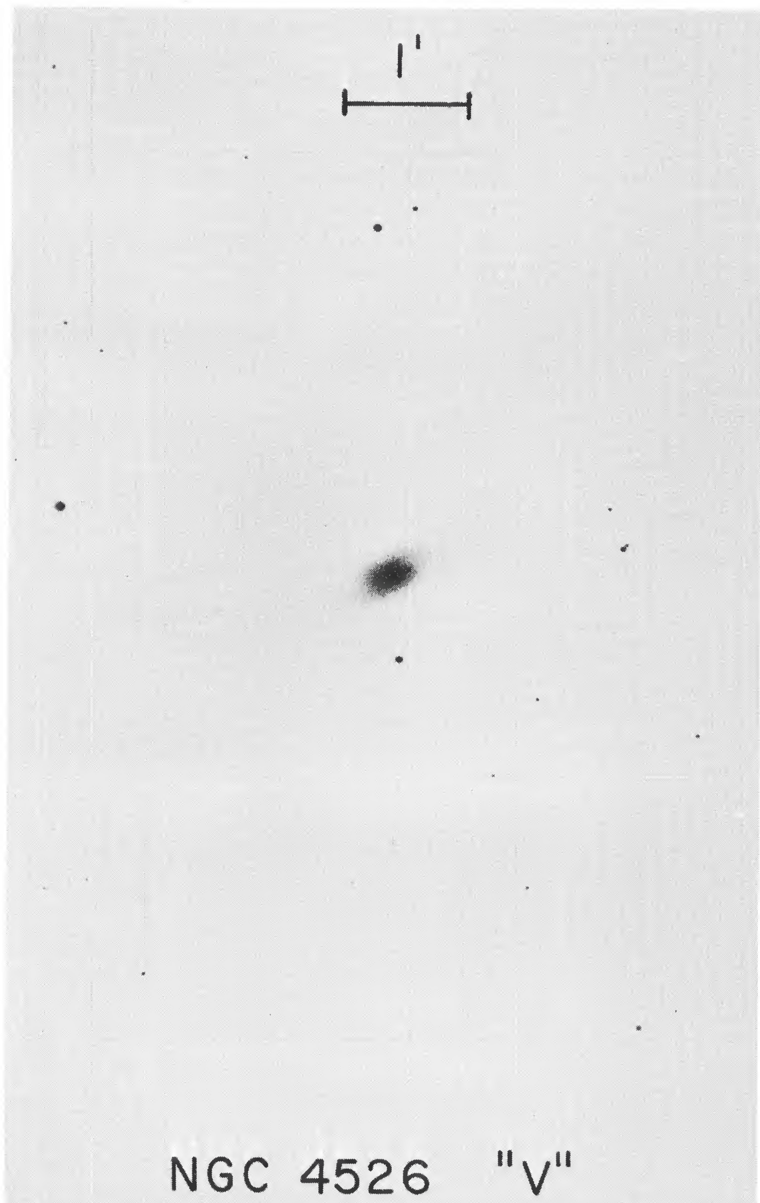

FIG. 4.—NGC 4526, from a 103a-D + GG 14 (Schott) filter (the V passband) taken with the Crossley; note the spiral-type distortions at a radius of about 30″.

BURSTEIN (*see* page 449)

VI. SUMMARY

Photographic surface photometry of 18 S0 galaxies and one elliptical, NGC 3379, is presented quantitatively in the form of major- and minor-axis profiles and qualitatively in the form of isophotal maps.

Comparison of the present photometry with the photometry of others points out large systematic errors in certain previous studies, namely, those of Fraser (1977), Benedict (1971), and Liller (1960, 1966). In particular, Liller's photometry is systematically fainter near the centers of galaxies, which leads one to seriously underestimate the amount of light in the bulge. The conclusions of Fraser (1977) regarding various galaxy parameters, as derived from his photometry, are likely to be seriously affected by the large systematic errors in his data.

The S0 disks in the present sample exhibit a variety of luminosity distributions, but almost all of these variations can be described in terms of a family of perturbations of an overall exponential profile that vary both in scale size and in amplitude.

Of the 16 "normal" S0's in this sample, four, or one-fourth, of the galaxies exhibit subtle nonaxisymmetric peculiarities in their disks. Since the selection bias in this sample was to select *against* peculiar galaxies, it seems that there are perhaps as many "peculiar" S0's as there are "normal" S0's. In this respect, one can categorize the S0 class as being made up of galaxies with a variety of different structures (cf. Freeman 1977).

The quantitative properties of both the bulges and the disks of "normal" S0's will be discussed in detail in forthcoming papers of this series.

My thanks and appreciation go to the director and the staff of the Hale Observatories, especially Dr. H. Arp, for the helpfulness and courteousness shown me while I was a guest observer. My special thanks go to the staff of the Lick Observatory, particularly Mr. Gene Harlan and Mr. Ron Laub, for their help during my many trips to Mount Hamilton. These data were initially reduced with the facilities of the UC Berkeley Astronomy Department, and the hospitality and graciousness of the faculty, graduate students, and staff of the Berkeley Astronomy Department are gratefully acknowledged.

The final data reductions were greatly helped by Mr. Robert Kibrick and Dr. Lloyd Robinson. Drs. R. Kron, A. Dressler, L. McDonald, and especially J. Kormendy provided many helpful and useful discussions during the course of this research. Thanks are also due to Dr. G. de Vaucouleurs, for a critical reading of an earlier version of this work and for supplying unpublished data. Special thanks go to Dr. I. King and Dr. M. F. Walker, for their help and advice throughout this work, and particularly to Dr. S. M. Faber, through whose careful and critical eye this work has been filtered.

This research was supported, in part, by NSF grant AST 76-08258.

REFERENCES

Baade, W., and Spitzer, L. 1951, *Ap. J.*, **113**, 413.
Balick, B., Faber, S. M., and Gallagher, J. S. 1976, *Ap. J.*, **209**, 710.
Barbon, R., Capaccioli, M., and Tarenghi, M. 1975, *Astr. Ap.*, **38**, 315.
Benedict, G. F. 1971, Ph.D. thesis, Northwestern University.
Binney, J., and Silk, J. 1978, *Comments Ap.*, **7**, 139.
Burkhead, M. S., and Kalinowski, J. K. 1974, *A.J.*, **79**, 835.
Burstein, D. 1978, Ph.D. thesis, University of California, Santa Cruz.
———. 1979, *AAS Photo-Bull.*, in press.
Burstein, D., Faber, S. M., and Gaskell, G. M. 1979, in preparation.
de Vaucouleurs, G. 1959, in *Handbuch der Physik*, Vol. **53**, ed. S. Flügge (Berlin: Springer-Verlag), p. 311.
———. 1968, *Appl. Optics*, **7**, 1513.
de Vaucouleurs, G., and de Vaucouleurs, A. 1964, *Reference Catalogue of Bright Galaxies* (Austin: University of Texas Press).
de Vaucouleurs, G., de Vaucouleurs, A., and Corwin, H. G. 1976, *Second Reference Catalogue of Bright Galaxies* (Austin: University of Texas Press) (RCBG II).
Dressel, L. L., and Condon, J. J. 1976, *Ap. J. Suppl.*, **31**, 187.
Eastman Kodak Co. 1973, *Kodak Plates and Films for Scientific Photography* (Kodak P-315).
Fraser, C. W. 1977, *Astr. Ap. Suppl.*, **29**, 161.
Freeman, K. C. 1970, *Ap. J.*, **160**, 811.
———. 1977, in *The Evolution of Galaxies and Stellar Populations*, ed. B. M. Tinsley and R. B. Larson (New Haven: Yale University Observatory), p. 157.
Gunn, J. E., and Gott, J. R. 1972, *Ap. J.*, **176**, 1.
Haynes, R. F., Huchtmeier, W. K. H., Siegman, B. C., and Wright, A. E. 1975, *A Compendium of Radio Measurements of Bright Galaxies* (Melbourne, Australia: CSIRO Division of Radiophysics).
Jones, W. B., Gallet, R. M., Obitts, D. L., and de Vaucouleurs, G. 1967, *Pub. Dept. Astr. Univ. Texas*, Ser. 2, Vol. **1**, No. 8.
King, I. R. 1978, *Ap. J.*, **222**, 1.
Kormendy, J. 1976, Ph.D. thesis, California Institute of Technology.
———. 1977, *Ap. J.*, **214**, 359.
Krumm, N. 1977, Ph.D. thesis, Cornell University.
Krumm, N., and Salpeter, E. E. 1976, *Ap. J.* (*Letters*), **208**, L7.
Liller, M. H. 1960, *Ap. J.*, **132**, 306.
———. 1966, *Ap. J.*, **146**, 28.
Markarian, B. E., Oganesian, E. Ya., and Arakelian, A. N. 1965, *Astrofizika*, **1**, 38.
Miller, R. H., and Prendergast, K. H. 1962, *Ap. J.*, **136**, 713.
Miller, W. C. 1971, *AAS Photo-Bull.*, **2**, 3.
Sandage, A. 1961, *Hubble Atlas of Galaxies* (Washington: Carnegie Institution of Washington).
Sandage, A., Freeman, K. C., and Stokes, N. R. 1970, *Ap. J.*, **160**, 831.
Sérsic, J. L. 1968, *Atlas de galaxias australes* (Córdoba: Observatorio Astronómico).
Strom, S. E., and Strom, K. E. 1978, in *IAU Symposium No. 77, Structure and Properties of Nearby Galaxies*, ed. E. M. Berkhuijsen and R. Wielebinski (Dordrecht: Reidel), p. 69.
Tsikoudi, V. 1977, Ph.D. thesis, University of Texas, Austin.
van den Bergh, S. 1976, *Ap. J.*, **206**, 883.
van Houten, C. J. 1961, *Bull. Astr. Inst. Netherlands*, **16**, 1.
Yoshizawa, M., and Wakamatsu, K. 1975, *Astr. Ap.*, **44**, 363.

David Burstein: Department of Terrestrial Magnetism, Carnegie Institution of Washington, 5241 Broad Branch Road, Northwest, Washington, DC 20015

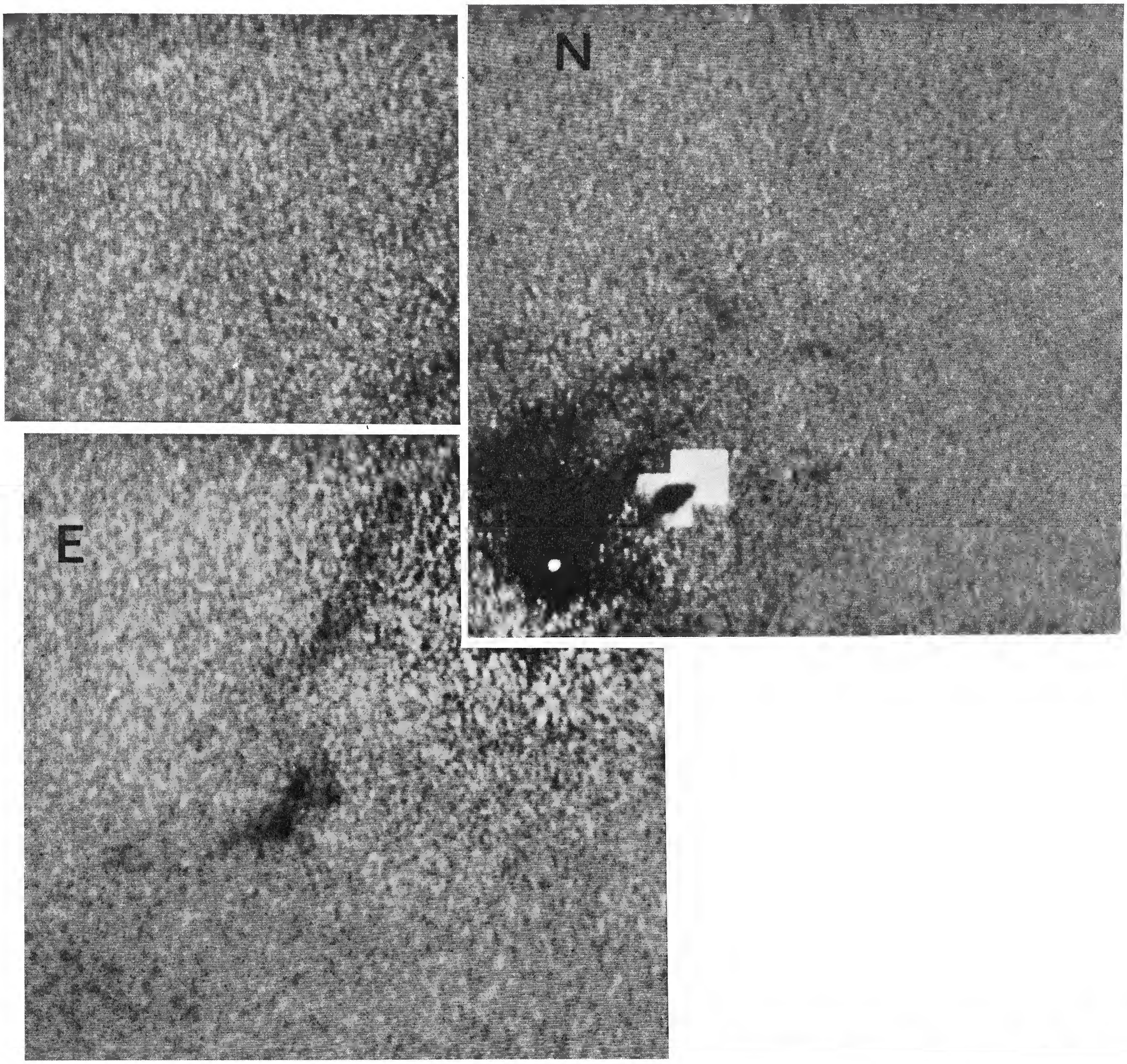

FIG. 3.—A montage of three Hα + [N II] video camera pictures of M87. The pictures were obtained 1978 January 13 at the f/8 Cassegrain focus of the 4 m telescope. Integration times for the northeast and southeast quadrants were 13 minutes each through the on-band (6593/48) and off-band (6075/175) filters, and for the northwest quadrant were 26 minutes each. The stellar continuum was removed from each picture by subtracting the off-band picture from the on-band picture. The Hα + [N II] emission regions are seen as black against the gray background. All the emission features seen in Figs. 1 and 2 can be seen here, as well as several faint new features. The optical nucleus of M87 is marked with a white dot, and the synchrotron jet has been reinserted into the picture in the two small overlapping windows. The borders between the pictures were purposely blackened to prevent any illustion of emission aligned with the borders.

FORD AND BUTCHER (*see* page 151)